

# Differential Recognition of CD1d- $\alpha$ -Galactosyl Ceramide by the V $\beta$ 8.2 and V $\beta$ 7 Semi-invariant NKT T Cell Receptors

Daniel G. Pellicci,<sup>1,5</sup> Onisha Patel,<sup>2,5</sup> Lars Kjer-Nielsen,<sup>1,5</sup> Siew Siew Pang,<sup>2</sup> Lucy C. Sullivan,<sup>1</sup> Konstantinos Kyriassoudis,<sup>1</sup> Andrew G. Brooks,<sup>1</sup> Hugh H. Reid,<sup>2</sup> Stephanie Gras,<sup>2</sup> Isabelle S. Lucet,<sup>2</sup> Ruide Koh,<sup>2</sup> Mark J. Smyth,<sup>3</sup> Thierry Mallevaey,<sup>4</sup> Jennifer L. Matsuda,<sup>4</sup> Laurent Gapin,<sup>4</sup> James McCluskey,<sup>1</sup> Dale I. Godfrey,<sup>1,6,\*</sup> and Jamie Rossjohn<sup>2,6,\*</sup>

<sup>1</sup>Department of Microbiology and Immunology, University of Melbourne, Parkville, Victoria 3010, Australia

<sup>2</sup>The Protein Crystallography Unit, ARC Centre of Excellence in Structural and Functional Microbial Genomics, Department of Biochemistry and Molecular Biology, School of Biomedical Sciences, Monash University, Clayton, Victoria 3800, Australia

<sup>3</sup>Peter MacCallum Cancer Centre, St. Andrews Place, East Melbourne, Victoria 3002, Australia

<sup>4</sup>Department of Immunology, University of Colorado Health Sciences Center and National Jewish Health, Denver, CO 80206, USA

<sup>5</sup>These authors contributed equally to this work

<sup>6</sup>These authors contributed equally to this work

\*Correspondence: [godfrey@unimelb.edu.au](mailto:godfrey@unimelb.edu.au) (D.I.G.), [jamie.rossjohn@med.monash.edu.au](mailto:jamie.rossjohn@med.monash.edu.au) (J.R.)

DOI 10.1016/j.immuni.2009.04.018

## SUMMARY

The semi-invariant natural killer T cell receptor (NKT TCR) recognizes CD1d-lipid antigens. Although the TCR $\alpha$  chain is typically invariant, the  $\beta$  chain expression is more diverse, where three V $\beta$  chains are commonly expressed in mice. We report the structures of V $\alpha$ 14-V $\beta$ 8.2 and V $\alpha$ 14-V $\beta$ 7 NKT TCRs in complex with CD1d- $\alpha$ -galactosylceramide ( $\alpha$ -GalCer) and the 2.5 Å structure of the human NKT TCR-CD1d- $\alpha$ -GalCer complex. Both V $\beta$ 8.2 and V $\beta$ 7 NKT TCRs and the human NKT TCR ligated CD1d- $\alpha$ -GalCer in a similar manner, highlighting the evolutionarily conserved interaction. However, differences within the V $\beta$  domains of the V $\beta$ 8.2 and V $\beta$ 7 NKT TCR-CD1d complexes resulted in altered TCR $\beta$ -CD1d-mediated contacts and modulated recognition mediated by the invariant  $\alpha$  chain. Mutagenesis studies revealed the differing contributions of V $\beta$ 8.2 and V $\beta$ 7 residues within the CDR2 $\beta$  loop in mediating contacts with CD1d. Collectively we provide a structural basis for the differential NKT TCR V $\beta$  usage in NKT cells.

## INTRODUCTION

Natural killer T (NKT) cells are a unique lymphocytic sublineage that recognize lipid-based antigens presented by CD1d, a major histocompatibility complex (MHC) class I-like antigen (Ag)-presenting molecule (Bendelac et al., 2007). NKT cells are implicated in a broad range of diseases, including microbial immunity, tumor immunity, autoimmunity, and allergy (Bendelac et al., 2007; Godfrey and Kronenberg, 2004; Matsuda et al., 2008). NKT cells are present in mice and humans, and typically express a semi-invariant T cell receptor (NKT TCR) consisting of an invariant TCR $\alpha$  chain (V $\alpha$ 24J $\alpha$ 18 in humans; V $\alpha$ 14J $\alpha$ 18 in mice), paired with a limited selection of TCR $\beta$  chains (V $\beta$ 11 in humans; V $\beta$ 8.2, V $\beta$ 7, or V $\beta$ 2 in mice) (Burdin et al., 1998; Godfrey et al., 2004;

Porcelli et al., 1993). The restricted NKT TCR repertoire is considered to reflect their recognition of the monomorphic CD1d molecule presenting glycolipid antigens. The crystal structure of a human NKT TCR-CD1d-glycolipid ( $\alpha$ -galactosylceramide;  $\alpha$ -GalCer) complex provided a snapshot into the basis of NKT recognition and revealed a markedly different mode of TCR recognition in comparison to that observed for TCR-MHC-peptide complexes (Borg et al., 2007). In contrast to the emerging generalities of the TCR-MHC-peptide interaction (Godfrey et al., 2008; Rudolph et al., 2006), the NKT TCR docked parallel to, and at the extreme end of, the CD1d-Ag binding cleft. Within this unusual NKT TCR-CD1d docking framework, interactions with CD1d were dominated by the complementarity determining region (CDR) 3 $\alpha$  loop encoded by J $\alpha$ 18 and V $\beta$ 11-encoded CDR2 $\beta$  loop, whereas the CDR1 $\alpha$  and CDR3 $\alpha$  loops contacted the  $\alpha$ -GalCer (Borg et al., 2007). Alanine-scanning mutagenesis studies in the human V $\beta$ 11 NKT TCR and mouse V $\beta$ 8.2 NKT TCR were consistent with this NKT TCR-CD1d- $\alpha$ -GalCer docking footprint (Scott-Browne et al., 2007; Wun et al., 2008), suggesting a remarkable conservation of this immune recognition event across the 70 million years of evolution that separate mice and humans. For instance, two tyrosine residues (Tyr48 $\beta$  and Tyr50 $\beta$ ) conserved in the human V $\beta$ 11 and mouse V $\beta$ 8.2 CDR2 $\beta$  loop were critical for NKT TCR-CD1d binding (Scott-Browne et al., 2007; Wun et al., 2008), suggesting that the V $\beta$ 8.2 NKT TCR docked in a very similar manner to that of the human NKT TCR, which was consistent with the reciprocal cross-species reactivity of these NKT TCRs (Brossay et al., 1998). Structural studies of  $\alpha$ -GalCer bound to human and mouse CD1d also revealed a broadly comparable landscape for NKT TCR binding (Koch et al., 2005; Zajonc et al., 2005), but nevertheless differences were apparent in the orientation of the  $\alpha$ -galactose head group presented by CD1d from the two different species (Godfrey et al., 2005). It is unclear how the NKT TCR would accommodate such differences when mediating cross-species reactivity. Moreover, it is just as unclear how different NKT TCRs might afford differential reactivity to the same or different glycolipid antigens.

It is established that NKT cells can see an array of different lipid-based antigens (reviewed in Bendelac et al., 2007;

Brutkiewicz, 2006; Godfrey et al., 2008), including bacteria-derived lipid antigens (Fischer et al., 2004; Kinjo et al., 2005, 2006; Mattner et al., 2005) and mammalian (self)-glycolipid antigens that include isoglobotrihexosylceramide (iGb3) (Zhou et al., 2004) and GD3 (Wu et al., 2003). Notably, with the exception of  $\alpha$ -GalCer, most other glycolipid antigens seem to be recognized with high affinity by only a subset of NKT cells (Brigl et al., 2006; Kinjo et al., 2006, 2008; Wu et al., 2003). For example, CD1d tetramers loaded with  $\alpha$ -diacylglycerol (Kinjo et al., 2006),  $\alpha$ -galacturonosylceramide (Kinjo et al., 2005), or GD3 (Wu et al., 2003) provided a spectrum of staining of NKT cells from negative to bright positive, whereas  $\alpha$ -GalCer-loaded CD1d tetramers stained the same population with uniformly high intensity (Kinjo et al., 2005, 2006; Wu et al., 2003). Similarly, iGb3 seems only to be able to stimulate a subset of  $\alpha$ -GalCer-reactive NKT cells (Brigl et al., 2006; Zhou et al., 2004). Although this suggests that antigen-specific subsets of NKT cells may exist, some NKT TCRs are nevertheless capable of recognizing several distinct glycolipid antigens similarly (Scott-Browne et al., 2007; Mallevaey et al., 2009 [this issue of *Immunity*]), albeit with varying affinity. Given that the NKT TCR $\alpha$  chain is invariant, this suggests that NKT TCR $\beta$  chain plays a role in determining thresholds of antigen reactivity and that this effectively enables some NKT TCRs to differentiate between antigens. This issue is particularly relevant to mouse NKT cells, which possess a more diverse TCR $\beta$  repertoire than humans, because of the frequent use of three V $\beta$  genes (V $\beta$ 8.2, V $\beta$ 7, and V $\beta$ 2), in which V $\beta$ 8.2- and V $\beta$ 7-containing NKT TCRs represent up to 80% of the mouse NKT cell repertoire. Although human NKT cells also exhibit some TCR $\beta$  chain diversity, only a small subset lack V $\beta$ 11 (Gadola et al., 2002), and furthermore, both human and mouse NKT cells have diverse CDR3 $\beta$  regions (Gadola et al., 2002; Matsuda et al., 2001). In the mouse NKT system, several studies support the differential contribution of TCR $\beta$  chains to recognition of different lipid based antigens:  $\alpha$ -GalCer is preferentially recognized by NKT cells bearing V $\beta$ 8.2 (Schumann et al., 2003), whereas iGb3 is preferentially recognized by NKT cells bearing V $\beta$ 7 (Schumann et al., 2006; Wei et al., 2006). Furthermore, although mutations in the CDR3 $\beta$  region of the mouse NKT TCR did not substantially affect  $\alpha$ -GalCer-mediated activation of NKT TCR-expressing hybridomas, they markedly influenced activation by other antigens, including iGb3 and GSL-1 (Scott-Browne et al., 2007). Thus, in order to understand how NKT cells can recognize glycolipid antigens, and the selective V $\beta$  gene usage by NKT cells, we need to gain a more complete picture of the different NKT TCRs in complex with CD1d-Ag.

Here we have determined the structures of the V $\beta$ 8.2 and V $\beta$ 7 NKT TCRs in complex with mouse CD1d- $\alpha$ -GalCer and compared them to a new 2.5 Å resolution structure of the human V $\beta$ 11 NKT TCR-CD1d- $\alpha$ -GalCer complex. Our findings, together with associated mutagenesis studies, provide insight into how the V $\beta$  repertoire of NKT TCRs impacts on CD1d-glycolipid recognition.

## RESULTS

### V $\beta$ 8.2 NKT TCR-CD1d- $\alpha$ -GalCer Complex

To begin to address the varied V $\beta$  usage in mouse NKT TCRs, we expressed and refolded the V $\alpha$ 14J $\alpha$ 18-V $\beta$ 8.2 and V $\alpha$ 14J $\alpha$ 18-

V $\beta$ 7 NKT TCRs (Figures S1A and S1B available online), then formed and crystallized the complex with the mouse (m)CD1d- $\alpha$ -GalCer. The structure of the V $\alpha$ 14J $\alpha$ 18-V $\beta$ 8.2 NKT TCR-mCD1d- $\alpha$ -GalCer complex was subsequently determined to 2.9 Å resolution to an  $R_{\text{fac}}$  and  $R_{\text{free}}$  of 23.4% and 29.8%, respectively (Table S1). The initial experimental phases clearly showed unbiased electron density for the  $\alpha$ -GalCer and moreover, apart from a small disordered (on account of mobility of the loop) region within the CDR3 $\beta$  loop (residues Gly98 $\beta$  to Glu105 $\beta$ ), the electron density at the V $\alpha$ 14-V $\beta$ 8.2 NKT TCR-mCD1d- $\alpha$ -GalCer interface was unambiguous.

Both the V $\beta$ 8.2 and V $\beta$ 7 NKT TCRs adopted an acute docking mode, binding approximately parallel to, and above, the F'-pocket of the CD1d-Ag binding cleft (Figures 1A–1D). The V $\beta$ 8.2 NKT TCR will be discussed first. This TCR interacted with mCD1d residues spanning 76–87 and 149–153 of the  $\alpha$ 1 helix and the  $\alpha$ 2 helix, respectively. The buried surface area (BSA) upon ligation was  $\approx 760$  Å<sup>2</sup>, in which the TCR $\alpha$  chain contributes nearly three times more BSA than the TCR $\beta$  chain (74% versus 26%, respectively) (Figure 1C), which is consistent with the  $\alpha$  chain dominating contacts with CD1d- $\alpha$ -GalCer in comparison to the  $\beta$  chain (Figure 2A; Table 1). The V $\beta$ 8.2 chain usage was dictated by the CDR2 $\beta$  loop interacting with mCD1d, as indicated by the fact that the CDR1 $\beta$  loop does not mediate any contacts with the Ag and the CDR3 $\beta$  loop was mobile (Table 1). The CDR2 $\beta$  loop formed a stretch of interactions exclusively with the  $\alpha$ 1 helix (residues 83–87) of mCD1d (Table 1; Figure 1C). Specifically, Tyr48 $\beta$  and Tyr50 $\beta$  formed H bonds and Van der Waals (VDW) contacts with Glu83 and Lys86 of CD1d, the latter of which formed a salt bridge with Glu56 $\beta$  (Figure 2B).

The V $\alpha$ 14-J $\alpha$ 18  $\alpha$  chain interactions were mediated via the CDR3 $\alpha$  and CDR1 $\alpha$  loops (57% and 17% BSA, respectively) (Figures 2A and 2C; Table 1). The CDR1 $\alpha$  loop interacted with  $\alpha$ -GalCer, whereas the J $\alpha$ 18-encoded CDR3 $\alpha$  loop interacted with mCD1d and  $\alpha$ -GalCer. The importance of the J $\alpha$ 18-encoded region is consistent with the lack of NKT cells in TCR J $\alpha$ 18 gene-inactivated mice (Cui et al., 1997). The CDR3 $\alpha$ -mediated interactions were largely electrostatic in nature, but also included some VDW-mediated contacts, including Leu99 $\alpha$  that sat in a small hydrophobic niche, formed by Leu84, Leu150, Val149 of mCD1d, but made contacts with only the latter residue (Figure 2A). There was an interdigitation of arginine residues at the CDR3 $\alpha$ -mCD1d interface, in which Arg79 from CD1d was flanked by Arg103 $\alpha$  and Arg95 $\alpha$ . This cluster of positively charged residues were dissipated by neighboring acidic groups, including Asp94 $\alpha$ , which salt bridged to Arg79; Arg103 $\alpha$  that salt bridged to Glu83; and Arg95 $\alpha$  that salt bridged to Asp80 (Figure 2A). Additionally, the main chain amide of Gly96 $\alpha$  H bonded to Asp153 of mCD1d and as such, all J $\alpha$ 18 residues at the tip of the CDR3 $\alpha$  loop, with the exception of Ala98 $\alpha$ , mediated contacts with mCD1d- $\alpha$ -GalCer (Table 1).

Only the galactose head group of  $\alpha$ -GalCer is exposed for recognition by the NKT TCR, and interacted solely with the CDR1 $\alpha$  and CDR3 $\alpha$  loops (Figure 2C; Table 1). The galactose ring sat below the CDR1 $\alpha$  loop and adjacent to the CDR3 $\alpha$  loop, forming VDW contacts on one face of the sugar ring with Arg95 $\alpha$ , Gly96 $\alpha$ , and Pro28 $\alpha$ . Arg95 $\alpha$  also made VDW contacts with the 3' hydroxyl of the sphingosine chain (Figure 2C).

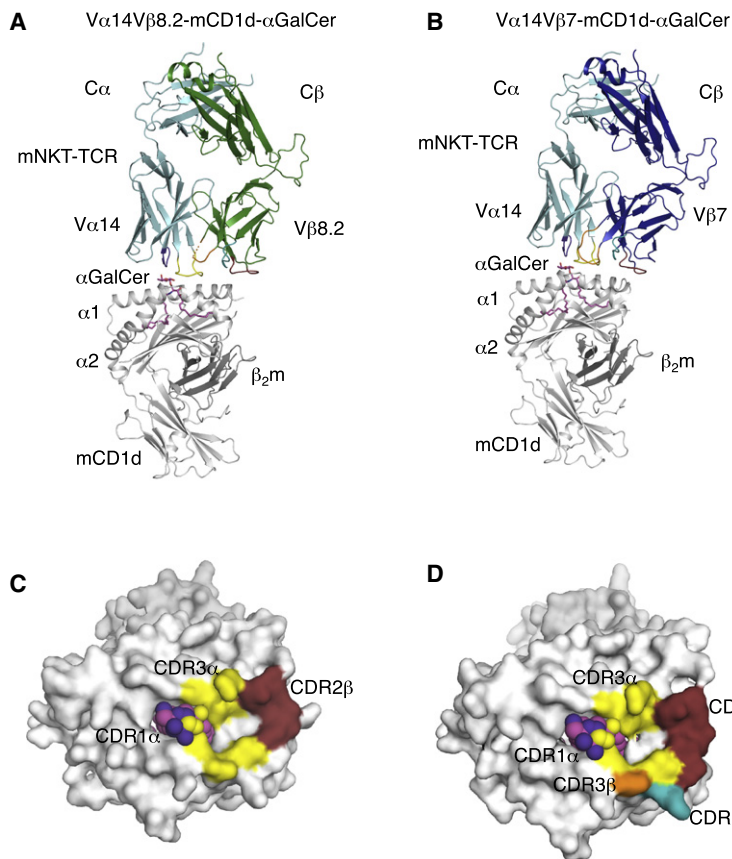


**Figure 1. Structure of Mouse NKT TCRs in Complex with Mouse CD1d- $\alpha$ -GalCer**

(A)  $V\alpha14$ - $V\beta8.2$  NKT TCR in complex with mCD1d- $\alpha$ -GalCer.  $\alpha$ -GalCer, magenta; mCD1d heterodimer, gray; TCR $\alpha$  chain, cyan;  $V\beta8.2$  NKT TCR $\beta$  chain, green; CDR1 $\alpha$ , purple; CDR3 $\alpha$ , yellow; CDR1 $\beta$ , teal; CDR2 $\beta$ , ruby; CDR3 $\beta$ , orange; mobile CDR3 $\beta$  region, dashed orange.

(B)  $V\alpha14$ - $V\beta7$  NKT TCR in complex with mouse CD1d- $\alpha$ -GalCer.  $V\beta7$  NKT TCR $\beta$  chain, blue; TCR $\alpha$  chain, mCD1d; CDR loops and  $\alpha$ -GalCer color coding as in (A).

(C) Footprint of the  $V\alpha14$ - $V\beta8.2$  NKT TCR on the surface of mouse CD1d- $\alpha$ -GalCer.  $\alpha$ -GalCer is shown in spheres. mCD1d,  $\alpha$ -GalCer, and CDR loops color coding as in (A).

(D) Footprint of the  $V\alpha14$ - $V\beta7$  NKT TCR on the surface of mCD1d- $\alpha$ -GalCer.  $\alpha$ -GalCer is shown in spheres. mCD1d,  $\alpha$ -GalCer, and CDR loops color coding as in (A).

Gly96 $\alpha$  H bonds to the 2' hydroxyl, whereas Asn30 $\alpha$  H bonds to both the 3' and 4' hydroxyl groups of the galactose ring. As such, the galactose ring is sequestered closely by the invariant  $\alpha$  chain of the  $V\beta8.2$  NKT TCR.

The crystal structure of the  $V\beta8.2$  NKT TCR-mCD1d- $\alpha$ -GalCer complex also allowed us to undertake precise structural corre-

lates of the alanine-scanning mutagenesis study previously conducted in this system (Scott-Browne et al., 2007). We can confirm that the effect of some of the  $V\beta8.2$  NKT TCR mutants in interacting with mCD1d- $\alpha$ -GalCer are due to indirect local effects (namely, CDR1 $\alpha$ : Val26Ala, Pro28Ala, Asn30Ala, His31Ala, Arg33Ala; CDR1 $\beta$ : Asn31Ala; CDR2 $\beta$ : Ser49Ala; Gly51Ala). In contrast, the mutational data are in accord with the crystal structure: namely the CDR1 $\alpha$ , CDR3 $\alpha$ , and CDR2 $\beta$  loops represent the energetic footprint of the interaction with mCD1d- $\alpha$ -GalCer. Accordingly, the structure of the  $V\beta8.2$  NKT TCR-mCD1d- $\alpha$ -GalCer complex provided a basis for understanding the biased gene usage of the semi-invariant  $V\alpha14J\alpha18$ - $V\beta8.2$  NKT TCR.

#### Conformational Changes upon Ligation

The mCD1d-PBS-25 (an analog of  $\alpha$ -GalCer with modifications in the lipid chains) and an engineered variant of  $V\alpha14J\alpha18$ - $V\beta8.2$

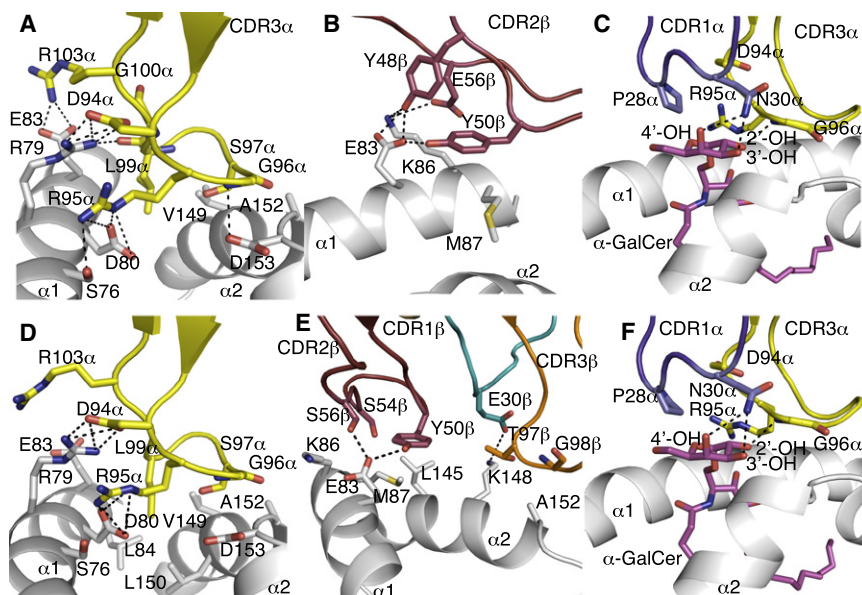


**Figure 2. Mouse CD1d and  $\alpha$ -GalCer Mediated Interactions with Mouse NKT TCRs**

CDR3 $\alpha$  mediates multiple contacts between mCD1d  $\alpha$  helices and  $\alpha$ -GalCer. CDR2 $\beta$  contacts  $\alpha1$  helix of mCD1d. CDR1 $\alpha$  interacts solely with  $\alpha$ -GalCer galactose head group. CDR1 $\beta$  mediates polar interactions with the  $\alpha2$  helix only in  $V\beta7$  NKT TCR-mCD1d- $\alpha$ -GalCer.

(A)  $V\beta8.2$  NKT TCR CDR3 $\alpha$  contacts with mCD1d. (B)  $V\beta8.2$  NKT TCR CDR2 $\beta$  contacts with mCD1d. (C)  $V\beta8.2$  NKT TCR CDR1 $\alpha$  and CDR3 $\alpha$  contacts with  $\alpha$ -GalCer.

(D)  $V\beta7$  NKT TCR CDR3 $\alpha$  contacts with mCD1d. (E)  $V\beta7$  NKT TCR CDR1 $\beta$ , CDR2 $\beta$ , and CDR3 $\beta$  contacts with mCD1d.

(F)  $V\beta7$  NKT TCR CDR1 $\alpha$  and CDR3 $\alpha$  contacts with  $\alpha$ -GalCer. CDR1 $\alpha$ , purple; CDR3 $\alpha$ , yellow; CDR1 $\beta$ , teal; CDR2 $\beta$ , ruby; CDR3 $\beta$ , orange;  $\alpha$ -GalCer, magenta; mCD1d, gray. H bond or salt bridge interactions are shown in black dashed lines.



**Table 1. Contacts at the mNKT TCR-mCD1d Interface**

CDR	V $\beta$ 8.2 NKT	mCD1d	Bond	V $\beta$ 7 NKT	mCD1d	Bond
CDR3 $\alpha$	Asp94 <sup>O<math>\delta</math>1</sup>	Arg79 <sup>N<math>\eta</math>1</sup> , Arg79 <sup>N<math>\eta</math>2</sup>	salt bridge	Asp94 <sup>O<math>\delta</math>1</sup>	same as V $\beta$ 8.2	
	Asp94 <sup>O<math>\delta</math>2</sup>	Arg79 <sup>N<math>\eta</math>1</sup> , Arg79 <sup>N<math>\eta</math>2</sup>	salt bridge	Asp94 <sup>O<math>\delta</math>2</sup>	same as V $\beta$ 8.2	
	Asp94	Arg79	VDW	Asp94	same as V $\beta$ 8.2	
	Arg95 <sup>N<math>\epsilon</math></sup>	Asp80 <sup>O<math>\delta</math>1</sup> , Asp80 <sup>O<math>\delta</math>2</sup>	salt bridge	Arg95 <sup>N<math>\epsilon</math></sup>	same as V $\beta$ 8.2	
	Arg95 <sup>N<math>\eta</math>1</sup>	Asp80 <sup>O<math>\delta</math>1</sup>	salt bridge	Arg95 <sup>N<math>\eta</math>1</sup>	Asp80 <sup>O<math>\delta</math>1</sup> , Asp80 <sup>O<math>\delta</math>2</sup>	salt bridge
		Ser76 <sup>O<math>\gamma</math></sup>	H bond			
	Arg95	Asp80, Arg79, Ser76	VDW	Arg95	same as V $\beta$ 8.2	
	Gly96 <sup>N</sup>	Asp153 <sup>O<math>\delta</math>2</sup>	H bond	Gly96 <sup>N</sup>	-	
	Gly96	Ala152, Asp153	VDW	Gly96	same as V $\beta$ 8.2	
	Ser97	Val149	VDW	Ser97	Val149, Ala152, Asp153	VDW
	Leu99	Arg79, Val149	VDW	Leu99	Arg79, Asp80, Glu83, Leu84, Val149, Leu150	VDW
	Leu99 <sup>o</sup>	Arg79 <sup>N<math>\eta</math>2</sup>	H bond	Leu99 <sup>o</sup>	-	
	Gly100	Arg79	VDW	Gly100	-	
	Arg103	Arg79, Glu83	VDW	Arg103	Arg79	VDW
	Arg103 <sup>N<math>\eta</math>1</sup>	Glu83 <sup>O<math>\epsilon</math>2</sup> , Glu83 <sup>O<math>\epsilon</math>1</sup>	salt bridge	Arg103 <sup>N<math>\eta</math>1</sup>	-	
CDR1 $\beta$	-			Glu30 <sup>O<math>\epsilon</math>2</sup>	Lys148 <sup>N<math>\epsilon</math></sup>	salt bridge
	-			Glu30	Lys148	VDW
CDR2 $\beta$	Tyr48 <sup>O<math>\eta</math></sup>	Glu83 <sup>O<math>\epsilon</math>1</sup> , Glu83 <sup>O<math>\epsilon</math>2</sup> , Lys86 <sup>N<math>\epsilon</math></sup>	H bond	-		
	Tyr48	Glu83, Lys86	VDW	-		
	Tyr50 <sup>O<math>\eta</math></sup>	Glu83 <sup>O<math>\epsilon</math>1</sup>	H bond	Tyr50 <sup>O<math>\eta</math></sup>	same as V $\beta$ 8.2	
	Tyr50	Glu83, Met87	VDW	Tyr50	same as V $\beta$ 8.2	
	-			Ser54	Met87, Leu145	VDW
	Glu56 <sup>O<math>\epsilon</math>1</sup>	Lys86 <sup>N<math>\epsilon</math></sup>	salt bridge	Ser56 <sup>O<math>\gamma</math></sup>	Glu83 <sup>O<math>\epsilon</math>1</sup>	H bond
	Glu56	Lys86	VDW	Ser56	Glu83, Lys86	VDW
CDR3 $\beta$	-			Thr97	Ala152	VDW
	-			Gly98	Ala152	VDW
CDR	V $\beta$ 8.2 NKT	$\alpha$ -GalCer	Bond	V $\beta$ 7 NKT	$\alpha$ -GalCer	Bond
CDR1 $\alpha$	Pro28	6'-OH <sup>G</sup> , 5'-O <sup>G</sup> , C-1 <sup>G</sup>	VDW	Pro28	same as V $\beta$ 8.2	
	Asn30	C-2 <sup>G</sup> , C-3 <sup>G</sup> , C-4 <sup>G</sup> , 3'-OH <sup>G</sup> , 4'-OH <sup>G</sup>	VDW	Asn30	-	
	Asn30 <sup>N<math>\delta</math>2</sup>	3'-OH <sup>G</sup> , 4'-OH <sup>G</sup>	H bond	Asn30 <sup>N<math>\delta</math>2</sup>	same as V $\beta$ 8.2	
CDR3 $\alpha$	Asp94 <sup>o</sup>	C-1 <sup>G</sup>	VDW	Asp94 <sup>o</sup>	same as V $\beta$ 8.2	
	Arg95	2'-OH <sup>G</sup> , C-2 <sup>G</sup> , 3'-OH <sup>S</sup>	VDW	Arg95	same as V $\beta$ 8.2	
	Gly96 <sup>N</sup>	2'-OH <sup>G</sup>	H bond	Gly96 <sup>N</sup>	same as V $\beta$ 8.2	
	Gly96	C-2 <sup>G</sup> , 3'-OH <sup>G</sup>	VDW	Gly96	C-2 <sup>G</sup> , 3'-OH <sup>G</sup> , 2'-OH <sup>G</sup>	VDW

Atomic contacts determined with the CCP4i implementation of CONTACT and a cutoff of 4.5 Å.

Van der Waals interactions defined as nonhydrogen bond contact distances of 4 Å or less.

Hydrogen bond interactions are defined as contact distances of 3.3 Å or less.

Salt bridge is defined as contact distance of 4.5 Å or less.

<sup>G</sup>= contacts with Galactose head group.

<sup>S</sup>= contacts with Sphingosine chain.

NKT TCR (which included mutations at the V $\alpha$ -V $\beta$  interface and within the invariant CDR3 $\alpha$  loop) have been solved in the nonliganded state (Zajonc et al., 2005, 2008). Hence we evaluated the degree of plasticity in this V $\beta$ 8.2 NKT TCR-mCD1d- $\alpha$ -GalCer interaction by comparing the elements of the complex in their liganded and unliganded state. The CDR loops of the V $\beta$ 8.2 NKT TCR did not change conformation appreciably upon ligation to mCD1d- $\alpha$ -GalCer, although movements in some side chains (Asn30 $\alpha$ , Tyr48 $\beta$ , and Tyr50 $\beta$ ) were observed (data not shown). Interestingly, upon V $\beta$ 8.2 NKT TCR ligation, the  $\alpha$ -GalCer head group was

observed to be shifted by approximately 1 Å (Figure S2). In comparison to the nonliganded V $\beta$ 8.2 NKT TCR (Zajonc et al., 2008), there was a slight change in the juxtapositioning (9.5°) of the V $\alpha$ 14 and V $\beta$ 8.2 domains upon ligation. Notably, such movements have been observed previously in TCR-pMHC interactions, where they are thought to relate to signal transmission (Ishizuka et al., 2008).

In addition, there was minimal movement in the mCD1d upon ligation, with some reorientation of side-chain conformations observed including Arg79, Glu83, Lys86, and Lys148 from

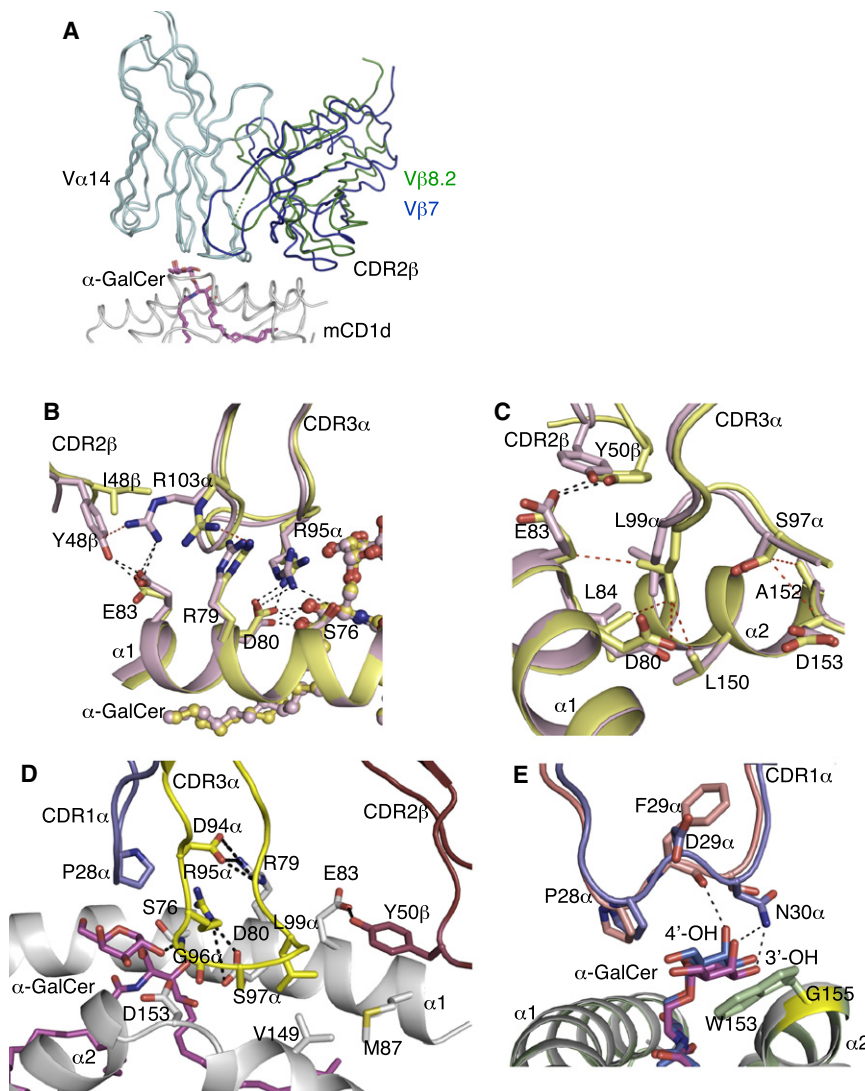


**Figure 3. Comparison of V $\alpha$ 14-V $\beta$ 8.2, V $\alpha$ 14-V $\beta$ 7, and V $\alpha$ 24-V $\beta$ 11 NKT TCR-mCD1d- $\alpha$ -GalCer Complexes**

(A) Superposition of V $\alpha$ 14-V $\beta$ 8.2 NKT TCR-mCD1d- $\alpha$ -GalCer and V $\alpha$ 14-V $\beta$ 7 NKT TCR-mCD1d- $\alpha$ -GalCer. Differences in the relative juxtapositioning of the V $\beta$ 8.2-V $\beta$ 7 and V $\alpha$ 14 domains. TCR $\alpha$  chain, cyan; V $\beta$ 8.2 NKT TCR $\beta$  chain, green; V $\beta$ 7 NKT TCR $\beta$  chain, blue;  $\alpha$ -GalCer, magenta; mCD1d, gray.

(B) Differences in the sequence of CDR2 $\beta$  in V $\beta$ 8.2 and V $\beta$ 7 NKT TCR affected the position of Arg103 $\alpha$  in the CDR3 $\alpha$  loop and subsequently altered positions and contacts of Arg79, Asp80, Ser76, and Arg95 $\alpha$ . V $\alpha$ 14-V $\beta$ 8.2 NKT TCR-mCD1d- $\alpha$ -GalCer, pink; V $\alpha$ 14-V $\beta$ 7 NKT TCR-mCD1d- $\alpha$ -GalCer, yellow.  $\alpha$ -GalCer is shown in ball and stick. H bond or salt bridge interactions are shown in black dashed lines, and VDW interactions are shown in red dashed lines.

(C) Altered position of Tyr50 $\beta$  in V $\beta$ 7 NKT TCR affected contacts made by Ser97 $\alpha$  and Leu99 $\alpha$  at the tip of CDR3 $\alpha$  with mCD1d. Color coding as in (B). H bonds are shown in black dashed lines and VDW interactions are shown in red dashed lines.

(D) Conserved interactions mediated by CDR1 $\alpha$ , CDR3 $\alpha$ , and CDR2 $\beta$  loops of the human and mouse NKT TCRs on the surface of CD1d and  $\alpha$ -GalCer. CDR1 $\alpha$ , purple; CDR2 $\beta$ , ruby; CDR3 $\alpha$ , yellow;  $\alpha$ -GalCer, magenta; CD1d, gray. The numbering shown on CD1d is according to the mouse CD1d. H bonds or salt bridge interactions are shown in black dashed lines.

(E) The shift in the position of the galactose head group of  $\alpha$ -GalCer between mouse and the human NKT TCR-CD1d- $\alpha$ -GalCer structures is due to the presence of a bulky tryptophan side chain in human CD1d (Trp153) in contrast to glycine (Gly155, shown in yellow) in mouse CD1d. Human CDR1 $\alpha$ , salmon; mouse CDR1 $\alpha$ , purple;  $\alpha$ -GalCer in human, marine;  $\alpha$ -GalCer in mouse, magenta; hCD1d, pale green; mCD1d, gray.

mCD1d (data not shown). Overall, the lack of conformational change upon V $\beta$ 8.2 NKT TCR-mCD1d- $\alpha$ -GalCer ligation, which was also observed in the human NKT TCR-CD1d- $\alpha$ -GalCer interaction (Borg et al., 2007; Kjer-Nielsen et al., 2006), typifies the innate characteristics of this interaction mediated by a relatively “rigid” receptor-ligand binding, whereas TCRs typically show a greater degree of plasticity upon ligation with pMHC.

#### V $\beta$ 7 NKT TCR-CD1d- $\alpha$ -GalCer Complex

The V $\alpha$ 14J $\alpha$ 18-V $\beta$ 7 NKT TCR is expressed by approximately 15%–20% of the mouse NKT T cell repertoire (Benlagha et al., 2000; Matsuda et al., 2000), and the V $\beta$ 7 and V $\beta$ 8.2 chains share 54% sequence identity, with sequence differences located in the CDR1 $\beta$  and CDR2 $\beta$  loops (Figure S3). Accordingly, we also aimed to understand how the V $\beta$ 7 NKT TCR interacted with mCD1d- $\alpha$ -GalCer. Hence, the refolded V $\alpha$ 14-V $\beta$ 7 NKT TCR (Figure S1) complexed to mCD1d- $\alpha$ -GalCer was crystallized and the structure determined to 2.8 Å resolution with an  $R_{\text{fac}}$  and  $R_{\text{free}}$  of 22.4% and 27.1%, respectively (Table S1). The initial

experimental phases clearly showed unbiased electron density for  $\alpha$ -GalCer, and the electron density at the V $\alpha$ 14-V $\beta$ 7 NKT TCR-mCD1d- $\alpha$ -GalCer interface was unambiguous.

Like the V $\beta$ 8.2 NKT TCR-CD1d- $\alpha$ -GalCer complex, the V $\alpha$ 14-V $\beta$ 7 NKT TCR was perched above the F'-pocket of the CD1d-Ag binding cleft, interacting with a similar stretch of residues on mCD1d (76–87 and 145–153) (Figures 1D and 2D–2F). The footprint of the two TCRs were very similar, with the V $\alpha$  contacts being dictated by the CDR1 $\alpha$  and CDR3 $\alpha$  loops, the former exclusively contacting  $\alpha$ -GalCer and the latter making substantial contacts with both mCD1d and  $\alpha$ -GalCer. However, within these common footprints, there were notable differences in the contacts made between the V $\beta$ 7 and V $\beta$ 8.2 NKT TCRs and CD1d- $\alpha$ -GalCer, attributable to sequence differences between the NKT TCRs and differing relative juxtapositioning of the V $\beta$ 8.2 and V $\beta$ 7 domains with respect to the V $\alpha$ 14 domains (Figures 3A and 3B). In turn, these differences also altered the nature of some of the V $\alpha$ 14-J $\alpha$ 18-mCD1d- $\alpha$ -GalCer interactions (Figures 3B and 3C; Table 1), despite the commonality of the invariant  $\alpha$  chain between the two NKT TCRs.

These differences manifested in a larger BSA between the V $\beta$ 7 NKT TCR and mCD1d ( $\approx 860 \text{ \AA}^2$ ; Figure 1D) than the corresponding V $\beta$ 8.2 NKT TCR-mCD1d- $\alpha$ -GalCer footprint (Figure 1C). This was attributable to a differing juxtapositioning of V $\alpha$ 14 and V $\beta$ 7 ( $9^\circ$ ) compared with that of V $\alpha$ 14-V $\beta$ 8.2 NKT TCR, which resulted in the V $\beta$ 7 domain being positioned closer to mCD1d (Figure 3A), and hence resulted in more contacts with CD1d when compared to the V $\beta$ 8.2 NKT TCR (Table 1). Consequently, the V $\alpha$ 14 chain contributes 59% BSA and the V $\beta$ 7 chain 41% BSA at the V $\beta$ 7 NKT TCR-CD1d- $\alpha$ -GalCer interface.

The V $\beta$ 7 chain interacted only with mCD1d, and although the majority of contacts were mediated via the CDR2 $\beta$  loop (27% BSA), the CDR3 $\beta$  (9% BSA) loop and surprisingly the CDR1 $\beta$  loop (3% BSA) also mediated contacts with mCD1d (Figure 1D). Specifically, as a result of the V $\beta$ 7 chain leaning more toward the mCD1d in comparison to V $\beta$ 8.2, this permitted a salt bridge to be formed between Glu30 $\beta$  (Asn30 $\beta$  in V $\beta$ 8.2) and Lys148 (Figure 2E). The interactions with the CDR3 $\beta$  loop were via Thr97 $\beta$  and Gly98 $\beta$ , both of which abutted against Ala152 of mCD1d, and this interaction presumably aided in stabilizing the CDR3 $\beta$  loop. The interactions with the V $\beta$ 7 CDR2 $\beta$  loop were featured by Tyr50 $\beta$ , which lay flat against Met87 of mCD1d, forming a H bond with Glu83, the latter of which also formed a H bond with Ser56 $\beta$  (Figure 2E). Although Tyr50 $\beta$  and its interactions with CD1d are conserved between V $\beta$ 7 and V $\beta$ 8.2, the relative position of Tyr50 $\beta$  varies in the two complexes (Figure 3C). In addition, Ser54 $\beta$  formed VDW interactions with Met87 and Leu145. The small side chains of Ser54 $\beta$  and Ser56 $\beta$  were able to contact mCD1d as a result of the CDR2 $\beta$  chain being closer to mCD1d when compared to the corresponding CDR2 $\beta$  loop of the V $\beta$ 8.2 chain (Figure 3A).

Structural differences at the V $\alpha$ 14-V $\beta$ 7 and V $\alpha$ 14-V $\beta$ 8.2 interfaces also “transmitted” to alterations in some of the V $\alpha$ 14-J $\alpha$ 18-mCD1d contacts (Figure 3B). Specifically, although many of the  $\alpha$  chain-mediated contacts were similar (Table 1), differences in J $\alpha$ 18-mediated contacts were observed at the tip of the CDR3 $\alpha$  loop, namely residues Asp94 $\alpha$ , Arg95 $\alpha$ , Gly96 $\alpha$ , Ser97 $\alpha$ , Leu99 $\alpha$ , and Arg103 $\alpha$ . First, these changes appeared to emanate from an altered contact between Arg103 $\alpha$  and the respective V $\beta$  chains. Thus, in the V $\beta$ 8.2 NKT TCR, Arg103 $\alpha$  stretches between the V $\alpha$ -V $\beta$  interface, with its guanadinium group being tethered by Tyr48 $\beta$ , which enabled Arg103 $\alpha$  to salt bridge to Glu83 of mCD1d. In V $\beta$ 7, however, position 48 is occupied by an Ile residue, which does not contact mCD1d, and moreover results in a loss of interaction with Arg103 $\alpha$ , causing Arg103 $\alpha$  to swing away from the V $\alpha$ -V $\beta$  interface and pack against Arg79 of mCD1d (Figure 3B). This in turn affects the conformation of Arg95 $\alpha$  and Asp80 of mCD1d, the latter of which H bonds to  $\alpha$ -GalCer in V $\beta$ 8.2 and V $\beta$ 7. The altered conformation of Arg95 $\alpha$  in V $\beta$ 7 NKT TCR resulted in loss of an H bond interaction with Ser76 of mCD1d (Table 1). Second, the altered position of Tyr50 $\beta$  in V $\beta$ 8.2 and V $\beta$ 7 NKT TCRs (Figure 3C) also pushed the tip of the CDR3 $\alpha$  loop away from CD1d, thereby altering the interactions this region made with mCD1d- $\alpha$ -GalCer (Table 1). For example, this change caused Leu99 $\alpha$  to sit differently within the hydrophobic mCD1d niche, which in turn results in Leu99 $\alpha$  and Ser97 $\alpha$  forming more VDW contacts in the V $\beta$ 7 NKT TCR when compared to the V $\beta$ 8.2 NKT TCR-mCD1d- $\alpha$ -GalCer interface (Figure 3C; Table 1).

Accordingly, although the overall V $\beta$ 8.2 and V $\beta$ 7 NKT TCR-mCD1d- $\alpha$ -GalCer structures were similar, the V $\beta$ 7 domain

played a more prominent role at the interface and also affected the invariant  $\alpha$  chain-CD1d contacts.

### Comparison to the Human NKT TCR-CD1d- $\alpha$ -GalCer Complex

Previously, we had determined the structure of the human NKT TCR-CD1d- $\alpha$ -GalCer complex to 3.2  $\text{\AA}$  resolution, making it challenging to accurately assign subtle structural changes that may be present between differing NKT TCR-CD1d-Ag complexes. Accordingly, the human NKT TCR-CD1d- $\alpha$ -GalCer complex was crystallized in a different space group to that originally reported (Borg et al., 2007) and the structure determined to 2.5  $\text{\AA}$  resolution with an  $R_{\text{fac}}$  and  $R_{\text{free}}$  of 21.6% and 27.9%, respectively (Table S1). We then compared the structure of the high-resolution human NKT TCR-CD1d- $\alpha$ -GalCer complex to the two mouse NKT TCR-CD1d- $\alpha$ -GalCer complexes to ascertain the evolutionarily conserved characteristics of the NKT TCR-CD1d innate interaction (Figure 3D; Figures S4A and S4B). Overall, the footprints of the human and mouse NKT TCRs were similar, especially between the homologous V $\beta$  domains (V $\beta$ 11 in humans and V $\beta$ 8.2 in mouse). Within this common footprint, the following interactions were conserved between the three complexes: Pro28 $\alpha$  to  $\alpha$ -GalCer; Asp94 $\alpha$  to  $\alpha$ -GalCer; Asp94 $\alpha$  to Arg79; Arg95 $\alpha$  to  $\alpha$ -GalCer; Arg95 $\alpha$  to Asp80, Arg79, and Ser76; Gly96 $\alpha$  to  $\alpha$ -GalCer; Gly96 $\alpha$  to Asp153 (Asp151 in human CD1d); Ser97 $\alpha$  to Val149 (Val147 in human CD1d); Leu99 $\alpha$  to Val149; and Tyr50 $\beta$  to Glu83 and Met87 (Figure 3D).

Nonetheless, a number of differences at the NKT TCR-CD1d interfaces between the three complexes were present, and these were attributable to (1) altered V $\alpha$ -V $\beta$  juxtapositioning (approximately  $13^\circ$  to  $15^\circ$  rotation between human and mouse NKT TCR-CD1d complexes), (2) sequence differences between the respective CDR loops that mediated CD1d and  $\alpha$ -GalCer recognition, and (3) structural differences between hCD1d and mCD1d, which included an altered positioning of the  $\alpha$ -GalCer galactose head group because of the presence of a neighboring Trp153 (Gly155 in mCD1d) in hCD1d (Godfrey et al., 2005). Nevertheless, the  $\alpha$ -galactose head group was sequestered to a similar extent in all three NKT TCR-CD1d- $\alpha$ -GalCer structures (Figures 3D and 3E), with the preservation of the H bond interactions to the 2', 3', and 4' hydroxyl groups.

Accordingly, the NKT TCR footprint on CD1d is broadly comparable across species, highlighting the evolutionarily conserved nature of this interaction. Nevertheless, differences at the NKT TCR-CD1d interfaces were observed, suggesting that a degree of malleability in NKT TCR-CD1d recognition plays a role in the reciprocal cross-species reactivity between the human and mouse NKT TCRs.

### V $\beta$ 7 and V $\beta$ 8.2 NKT TCR Binding Affinity

Given the differences in the binding of the human NKT TCR and the mouse V $\beta$ 8.2 and V $\beta$ 7 NKT TCRs, we determined the affinity and relative avidity of the interactions by using surface plasmon resonance (SPR) and CD1d- $\alpha$ -GalCer tetramer inhibition studies, respectively.

The affinity (equilibrium dissociation constant,  $K_D$ ) of V $\beta$ 8.2 NKT TCR for mCD1d- $\alpha$ -GalCer was 70 nM, whereas the  $K_D$  for the V $\beta$ 7 NKT TCR-mCD1d- $\alpha$ -GalCer interaction was at 0.3  $\mu\text{M}$  (Figures 4A and 4C; Table S2). These differing affinities were

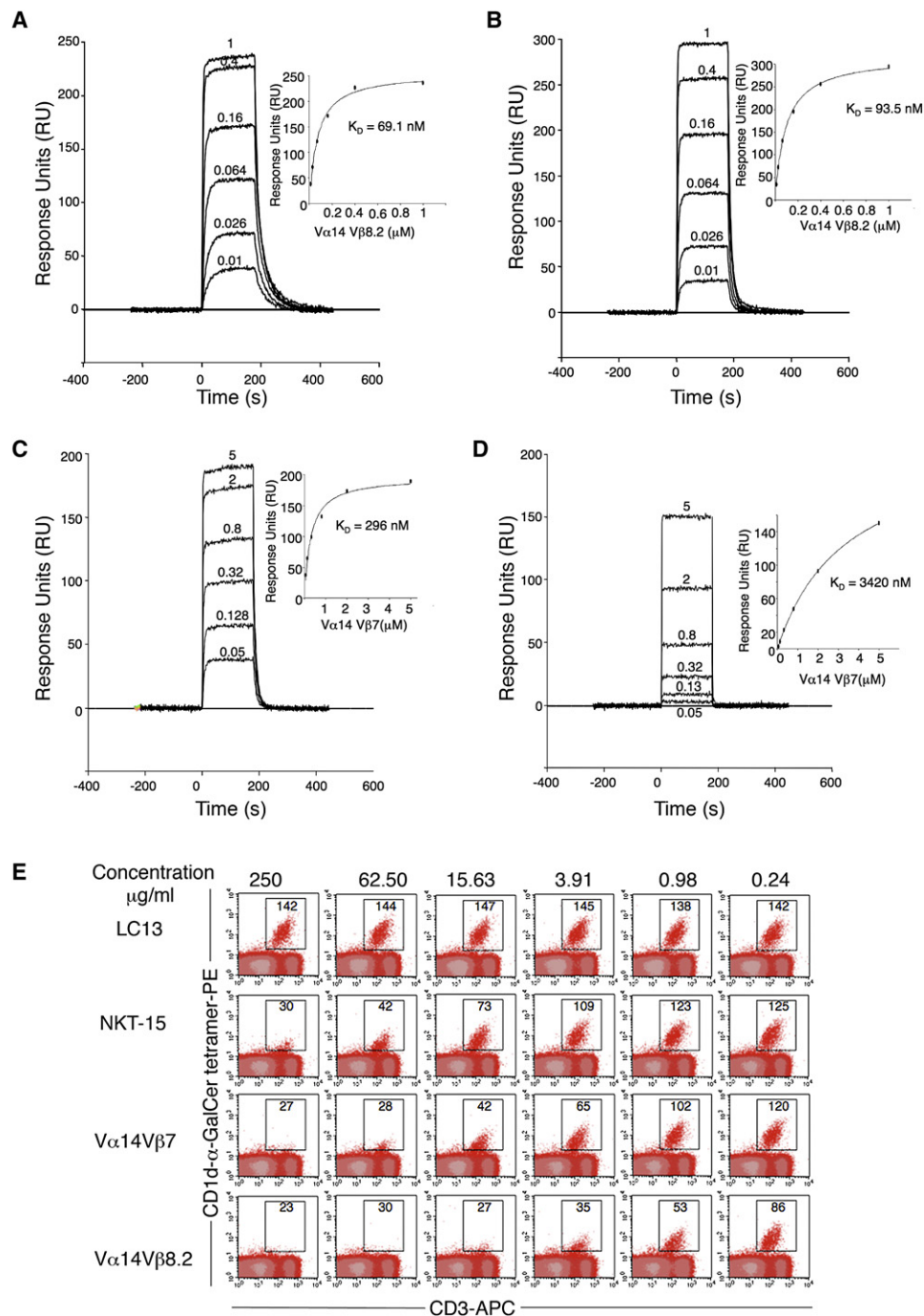


**Figure 4. Differential Binding Affinities of NKT TCRs to CD1d- $\alpha$ -GalCer**

(A–D)  $V\alpha 14J\alpha 18-V\beta 8.2$  (A and B) and  $V\alpha 14J\alpha 18-V\beta 7$  (C and D) NKT TCR were injected over streptavidin-immobilized mouse (A and C) and human (B and D) CD1d- $\alpha$ -GalCer and simultaneously over a control cell coated with unloaded CD1d. Sensorgrams show the binding (response units, RU) of increasing concentrations of TCR (0.01 to 1  $\mu$ M for  $V\alpha 14J\alpha 18-V\beta 8.2$  and 0.05 to 5  $\mu$ M for  $V\alpha 14J\alpha 18-V\beta 7$ ) to mouse and human CD1d- $\alpha$ -GalCer after baseline subtraction. Insets show saturation plots demonstrating equilibrium binding of NKT TCR to immobilized CD1d- $\alpha$ -GalCer. The equilibrium dissociation constants ( $K_D$ ) derived by equilibrium analysis were equivalent to those derived by kinetic analysis.

(E) CD1d- $\alpha$ -GalCer tetramer inhibition. Recombinant soluble NKT TCRs were examined for their ability to block binding of mCD1d- $\alpha$ -GalCer tetramers to mouse NKT cells. PE-labeled CD1d- $\alpha$ -GalCer tetramers were preincubated with titrating amounts of soluble NKT TCRs or an irrelevant TCR control, LC13, before staining of mouse thymocytes. Cells were analyzed by flow cytometry showing mCD1d- $\alpha$ -GalCer tetramer-PE on the vertical axis and anti-CD3 APC on the horizontal axis. CD3<sup>+</sup> mCD1d- $\alpha$ -GalCer tetramer<sup>+</sup> thymic NKT cells are indicated within the square with the MFI (mean fluorescence intensity) indicated. All measurements were taken in duplicate.



attributable to much longer half life of the V $\beta$ 8.2 NKT TCR ( $t_{1/2}$  = 17.3 s) compared to the V $\beta$ 7 NKT TCR ( $t_{1/2}$  = 6.9 s) and were consistent with previous affinity measurements determined via CD1d-multimer staining (Mallevaey et al., 2009; Schumann et al., 2003). Consistent with the reciprocal cross-species reactivity of NKT cells, the V $\beta$ 8.2 NKT TCR also bound human (h)CD1d- $\alpha$ -GalCer ( $K_D$   $\approx$  94 nM) with similar affinity to mCD1d- $\alpha$ -GalCer, although the respective on and off rates were distinct (Figures 4A and 4B; Table S2). In contrast, the V $\beta$ 7 NKT TCR bound hCD1d- $\alpha$ -GalCer with approximately 12-fold lower affinity ( $K_D$   $\approx$  3.4  $\mu$ M; Figure 4D), which was consistent with hCD1d- $\alpha$ -GalCer dimer preferentially detecting V $\beta$ 8.2 NKT cells (Schumann et al., 2003). Human NKT TCR affinity for hCD1d- $\alpha$ -GalCer was lower ( $K_D$   $\approx$  0.2  $\mu$ M) than that for the V $\beta$ 8.2 NKT TCR-mCD1d- $\alpha$ -GalCer interaction (Table S2), and human NKT TCR bound with moderately lower affinity to mCD1d- $\alpha$ -GalCer ( $K_D$   $\approx$  1  $\mu$ M), as observed previously (Wun et al., 2008).

To cross-validate the binding affinity for the three NKT TCRs, we used a CD1d- $\alpha$ -GalCer tetramer binding inhibition assay (Figure 4E; Kjer-Nielsen et al., 2006). The V $\beta$ 8.2 NKT TCR blocked tetramer binding with the highest efficiency, still readily detectable to a concentration of 0.98  $\mu$ g/ml. In contrast, the V $\beta$ 7 NKT TCR was approximately 25% less effective and human NKT TCR was 25% less effective again. This hierarchy is consistent with the affinities of the different TCRs as determined by SPR analysis. The negative control TCR, LC13 (anti-HLA-B8-FLR) (Kjer-Nielsen et al., 2003), did not inhibit tetramer staining at any of the doses tested.

Accordingly, these data are consistent with our SPR affinity measurements, showing that V $\beta$ 8.2 NKT TCR preferentially interacts with CD1d- $\alpha$ -GalCer when compared to V $\beta$ 7 NKT TCR.

### NKT TCR Mutagenesis

Given the differing contacts made by the CDR2 $\beta$  loop of the V $\beta$ 8.2 and V $\beta$ 7 NKT TCRs, we next established the importance of the residues within these loops of the respective mouse NKT TCRs. With the structures as a guide, we mutated CDR2 $\beta$  residues that were observed to contact CD1d and examined the effect of the mutants via SPR (Figures 5A–5F; Table S3) and CD1d- $\alpha$ -GalCer tetramer inhibition studies (Figure 6). For the V $\beta$ 8.2 and V $\beta$ 7 NKT TCRs, three (Tyr48 $\beta$ Phe, Tyr50 $\beta$ Phe, Glu56 $\beta$ Ala) and four (Tyr50 $\beta$ Phe, Ser54 $\beta$ Ala, Ser56 $\beta$ Ala, Glu57 $\beta$ Ala) mutants from the CDR2 $\beta$  loop were examined, respectively, and one residue from the CDR1 $\beta$  loop served as a negative control (V $\beta$ 8.2, Asn28 $\beta$ Ala; V $\beta$ 7, Asp26 $\beta$ Ala). All of the mutant NKT TCR proteins behaved similarly to the WT NKT TCR in gel filtration and analysis under reducing and nonreducing SDS-PAGE. Furthermore, an ELISA study showed that the NKT TCR mutant proteins were as reactive as the WT NKT TCR to conformation-sensitive mAb reactive against the NKT TCR (data not shown). NKT TCR substitutions that caused <50% change in the affinity of the interaction with CD1d- $\alpha$ -GalCer compared to WT NKT TCR were considered to have no major effect. Conversely, NKT TCR substitutions that caused >50% change in binding affinity were considered to be energetically important to the interaction. As expected, the control mutations within the CDR1 $\beta$  loop did not affect CD1d- $\alpha$ -GalCer binding (Figures 5E, 5F, and 6). In the V $\beta$ 8.2 NKT TCR, the Tyr48 $\beta$ Phe, Tyr50 $\beta$ Phe, and Glu56 $\beta$ Ala mutants impacted substantially on CD1d- $\alpha$ -GalCer recognition,

consistent with previous alanine-scanning mutagenesis at positions 48 and 50 in the human V $\beta$ 11 NKT TCR, although the corresponding Glu56 $\beta$  position was shown not to be essential for the human NKT TCR-CD1d- $\alpha$ -GalCer interaction. The conservative Tyr48 $\beta$ Phe and Tyr50 $\beta$ Phe mutations revealed the importance of their hydroxyl groups in mediating a series of polar contacts with CD1d. In the V $\beta$ 7 NKT TCR, Ser56 $\beta$  and Glu57 $\beta$  were shown not to be critical for the interaction, whereas Tyr50 $\beta$  was shown to play a major role in the interaction with CD1d, again highlighting the importance of the aromatic residues in the CDR2 $\beta$  loop in mediating CD1d contacts. Interestingly, the Ser54 $\beta$ Ala mutation in the V $\beta$ 7 TCR was observed to markedly improve the affinity of the interaction from 134 to 32.6 nM, making the affinity of this mutant comparable to that of the wild-type V $\beta$ 8.2 NKT TCR. A similar result was observed in another study where CD1d tetramer binding was used to determine TCR affinity (Mallevaey et al., 2009). The effect of the Ser54 $\beta$ Ala mutant can be attributable to the Ser54 $\beta$  group being uncompensated within a hydrophobic pocket (Table 1), and accordingly, the Ala mutant forms more favorable VDW interactions when compared to the wild-type counterpart. Thus, not all residues within the CDR2 $\beta$  loop of the V $\beta$ 7 NKT TCR are of the optimal chemistry and composition to interact with CD1d, and this, in part, may explain why the V $\beta$ 8.2 NKT TCR interacts with CD1d- $\alpha$ -GalCer with a higher affinity when compared to the V $\beta$ 7 NKT TCR.

### DISCUSSION

The V $\beta$ 8.2 and V $\beta$ 7 NKT TCR-mCD1d- $\alpha$ -GalCer structures, in conjunction with the human NKT TCR-CD1d- $\alpha$ -GalCer structure, broadly supports earlier suggestions that the NKT TCR exhibits characteristics of a pattern-recognition receptor (Scott-Browne et al., 2007). Namely, the relatively rigid semi-invariant NKT TCR interacts with a monomorphic Ag-presenting molecule in an approximately conserved manner. Within this conserved docking framework that was situated above the CD1d F' pocket, the invariant CDR1 $\alpha$  loop and CDR3 $\alpha$  loop contact  $\alpha$ -GalCer and CD1d- $\alpha$ -GalCer, respectively, whereas the V $\beta$  domain interacted exclusively with CD1d. Although the NKT TCR is “innate-like,” the NKT TCR V $\beta$  chain nevertheless exhibits diversity in the CDR3 $\beta$  loop and the mouse NKT cell repertoire uses V $\beta$ 8.2, V $\beta$ 7, and to a lesser extent V $\beta$ 2 (Benlagha et al., 2000; Matsuda et al., 2000). Our study addressed the basis and impact of this differential V $\beta$  usage when recognizing the prototypic NKT cell Ag,  $\alpha$ -GalCer. The V $\beta$ 8.2 and V $\beta$ 7 NKT TCRs interacted with CD1d in a different manner as a result of sequence and structural differences between these V $\beta$  domains. These differences resulted in a greater involvement of the V $\beta$ 7 chain interacting with mCD1d when compared to the V $\beta$ 8.2 chain, which included the CDR1 $\beta$  loop of V $\beta$ 7-mediating contacts with CD1d. In addition, the importance of specific residues, as directly judged by mutagenesis data, within the respective CDR2 $\beta$  loops varied: in V $\beta$ 8.2 NKT TCR, Tyr48 $\beta$ , Tyr50 $\beta$ , and Glu56 $\beta$  were essential, whereas only Tyr50 $\beta$  was critical in V $\beta$ 7-mediated recognition of CD1d. Surprisingly, the Ser54 $\beta$ Ala mutant improved the affinity of the V $\beta$ 7 NKT TCR-CD1d- $\alpha$ -GalCer interaction markedly, thereby revealing simultaneously that the sequence and composition of the NKT TCR V $\beta$ 7 CDR2 $\beta$  loop is nonideal for interacting with CD1d, thereby providing insight into why the



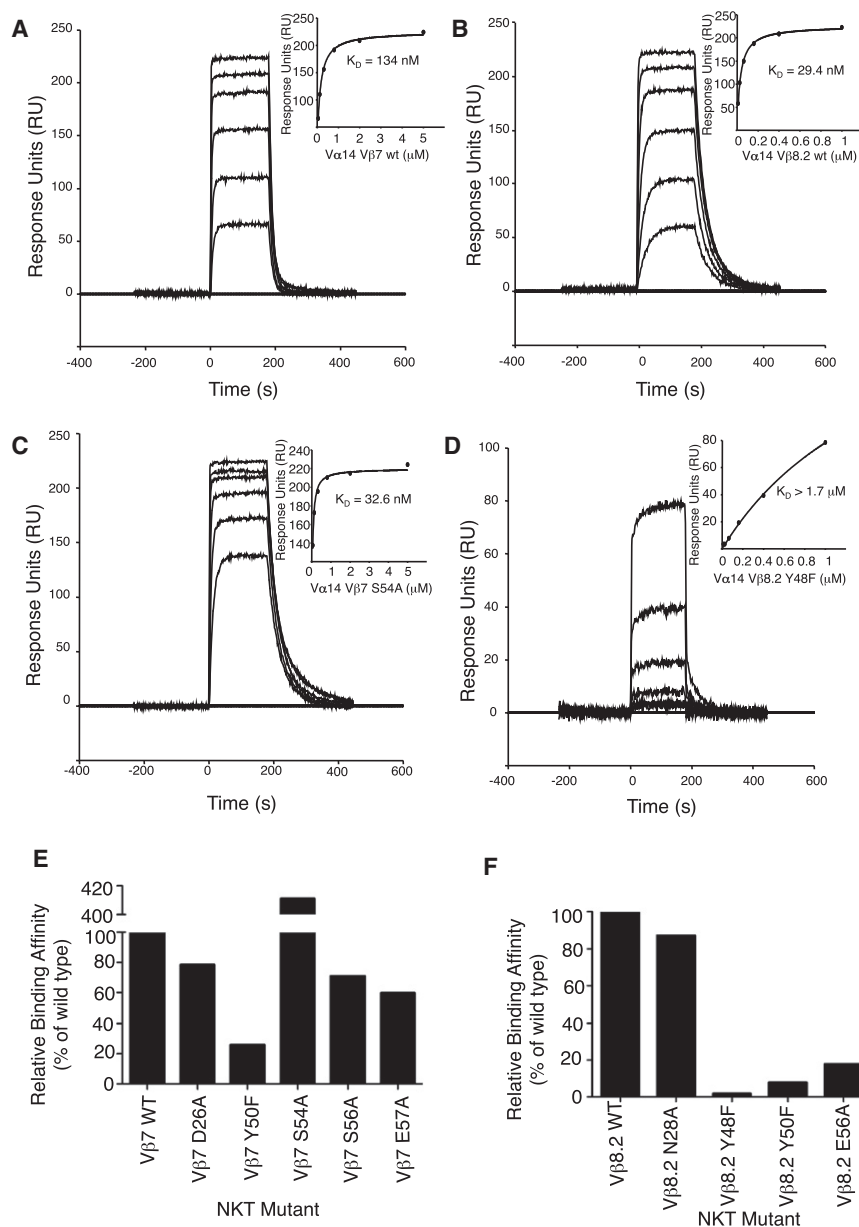


**Figure 5. Binding of Mutant NKT TCRs to Mouse CD1d- $\alpha$ -GalCer as Assessed by Surface Plasmon Resonance**

(A–D) Wild-type V $\beta$ 7 NKT TCR (A), V $\beta$ 8.2 NKT TCR (B), mutant V $\beta$ 7 NKT TCR S54A (C), and mutant V $\beta$ 8.2 (Y48F) NKT TCR (D) were injected over streptavidin-immobilized mouse CD1d- $\alpha$ -GalCer and over a control cell containing unloaded CD1d. Sensograms show the binding (response units, RU) of decreasing concentrations of TCR (5, 2, 0.8, 0.32, 0.13, and 0.05 for V $\alpha$ 14J $\alpha$ 18-V $\beta$ 7 TCRs and 1, 0.4, 0.16, 0.064, 0.026, and 0.01  $\mu$ M for V $\alpha$ 14J $\alpha$ 18-V $\beta$ 8.2 TCRs) to mouse CD1d- $\alpha$ -GalCer after subtraction of the control flow cell. Insets show saturation plots demonstrating equilibrium binding of NKT TCR to immobilized CD1d- $\alpha$ -GalCer.

(E and F) Binding of mutant NKT TCR to mouse CD1d  $\alpha$ -GalCer. Site-directed mutants of individual V $\beta$ 7 or V $\beta$ 8.2 residues were refolded with the invariant  $\alpha$  chain. The data are presented as a percentage binding of wild-type NKT TCR. Experiments were conducted in duplicate for the wild-type and for the following mutants: V $\beta$ 7 S54A, S56A, E57A, and V $\beta$ 8.2 N28A.

not contain any tyrosine residues, this indicates the evolutionary conserved “interaction codon” that underlies CD1d-restricted  $\alpha$ -GalCer recognition by the NKT TCR is encoded by the V $\alpha$ 14-J $\alpha$ 18 domain (V $\alpha$ 24-J $\alpha$ 18 in humans). Recently, conserved binding residues or “interaction codons” have been defined for V $\beta$ 8.2 TCRs ligating pMHC (Dai et al., 2008; Feng et al., 2007). This observation allows us to assess whether these residues adopt similar roles in MHC-restricted and CD1d-restricted recognition by V $\beta$ 8.2 TCRs. Whereas the two Tyr residues forming “interaction codons” within the CDR2 $\beta$  loop of V $\beta$ 8.2 TCRs are used in recognizing both MHC (Dai et al., 2008; Feng et al., 2007) and CD1d (Scott-Browne et al., 2007), they interact in markedly different regions of these Ag-presenting molecules (Godfrey et al., 2008), thereby highlighting the contrasting characteristics of peptide- and glycolipid-mediated recognition.

Despite the restricted NKT TCR repertoire, NKT cells can recognize a large array of CD1d-restricted lipid antigens (reviewed in Bendelac et al., 2007; Brutkiewicz, 2006). Given that the V $\beta$  domains can modulate the affinity for CD1d-Ags (Malle-vaey et al., 2009), this suggests that any given V $\beta$  chain will be an important factor in determining the range of Ags in which any given NKT TCR can interact with. The structural differences observed in the V $\beta$ 8.2 and V $\beta$ 7 NKT TCR recognition of mCD1d- $\alpha$ -GalCer may contribute to modulating the affinity toward other CD1d-restricted Ags. Moreover, the differences in CDR3 $\beta$  sequence, structure, and their potential for interaction with CD1d in the NKT TCR-CD1d- $\alpha$ -GalCer complexes indicate that

V $\beta$ 8.2 NKT TCR interacts with CD1d- $\alpha$ -GalCer with higher affinity than does V $\beta$ 7 NKT TCR. Furthermore, despite the invariant nature of V $\alpha$ 14-J $\alpha$ 18, differences in the V $\beta$  domains were “transferred” to the J $\alpha$ 18 chain, which impacted on J $\alpha$ 18-mediated CD1d- $\alpha$ -GalCer recognition. Collectively, these differences manifested in the V $\beta$ 8.2 NKT TCR interacting with mCD1d- $\alpha$ -GalCer with a moderately higher affinity compared to the V $\beta$ 7 NKT TCR.

The two mouse NKT TCR-CD1d- $\alpha$ -GalCer complexes, together with the 2.5 Å human NKT TCR-CD1d- $\alpha$ -GalCer structure reported here, allowed us to evaluate the residues in this interaction that are evolutionarily conserved. Namely, the conserved NKT TCR residues that contact identical residues in CD1d are Pro28 $\alpha$  of the CDR1 $\alpha$  loop; Asp94 $\alpha$ , Arg95 $\alpha$ , Gly96 $\alpha$ , Ser97 $\alpha$ , and Leu99 $\alpha$  of the CDR3 $\alpha$  loop; and Tyr50 $\beta$  of the CDR2 $\beta$  loop. However, given that the CDR2 $\beta$  loop of V $\beta$ 2 does

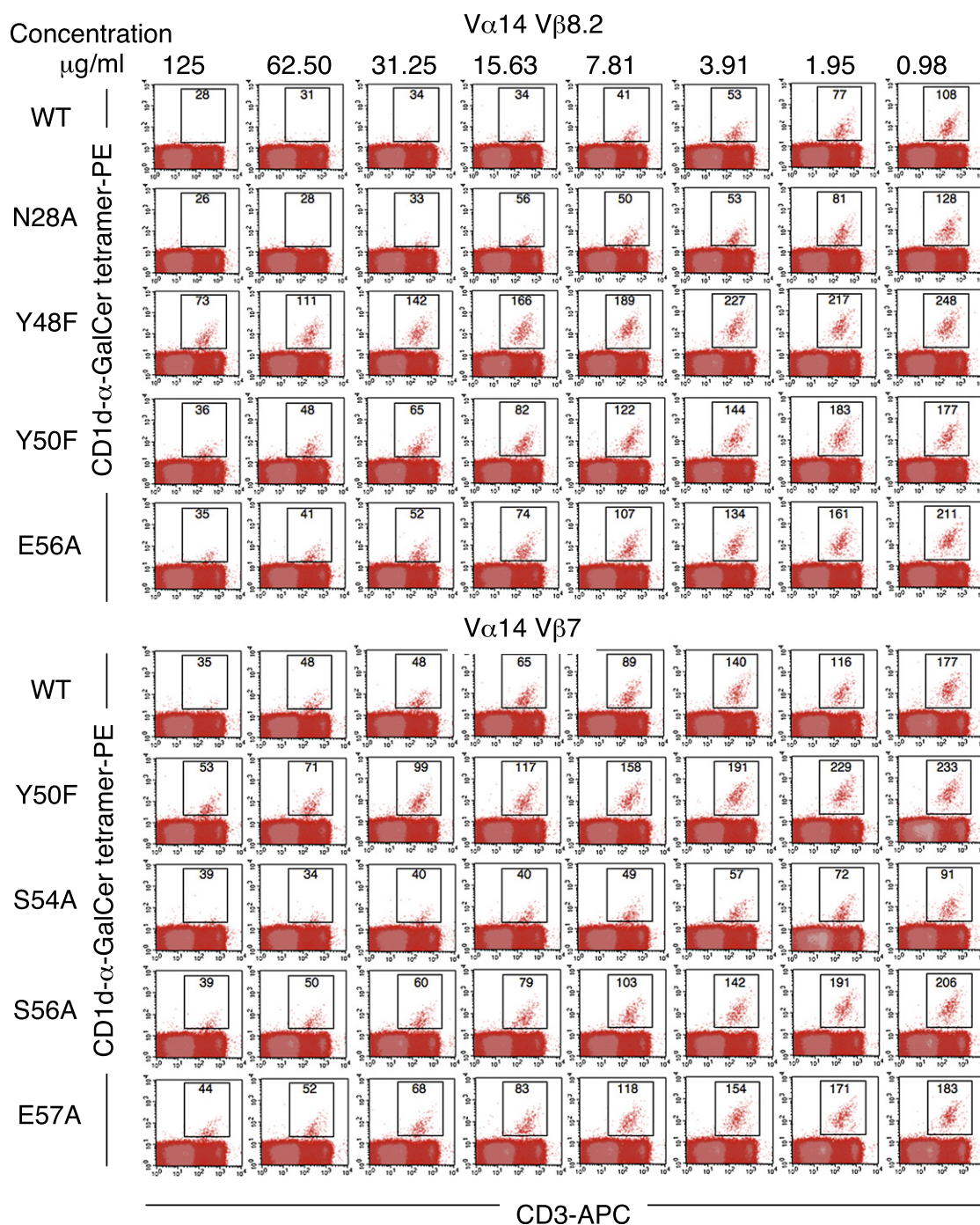


**Figure 6. Binding of Mutant NKT TCRs as Assessed by CD1d- $\alpha$ -GalCer Tetramer Inhibition**

Recombinant soluble NKT TCRs, and mutants thereof, were examined for their ability to block binding of mCD1d- $\alpha$ -GalCer tetramers to mouse NKT cells. PE-labeled CD1d- $\alpha$ -GalCer tetramers were preincubated with titrating amounts of soluble wild-type and mutant NKT TCRs before staining of mouse thymocytes. Cells were analyzed by flow cytometry showing mCD1d- $\alpha$ -GalCer tetramer-PE on the vertical axis and anti-CD3 APC on the horizontal axis. CD3<sup>+</sup> mCD1d- $\alpha$ -GalCer tetramer<sup>+</sup> thymic NKT cells are indicated within the square with the MFI indicated.

they may also play a role in fine-tuning the response to CD1d-Ag. Consistent with this,  $V\beta 8.2^+$  NKT TCRs were shown to have higher affinity for  $\alpha$ -GalCer bound to mCD1d, whereas  $V\beta 7^+$  NKT TCRs have been reported to preferentially recognize iGb3 when compared to  $V\beta 8.2$  NKT TCRs (Schumann et al., 2006;

Wei et al., 2006). However, the recent study (Mallevaey et al., 2009) found that hybridomas expressing  $V\beta 8.2$  NKT TCRs recognize CD1d-iGb3 with higher affinity than those expressing  $V\beta 7$  NKT TCRs. This discrepancy might, at least in part, indicate a key contribution by CDR3 $\beta$  regions to the recognition of iGb3

by V $\beta$ 7<sup>+</sup> NKT cells selected in vivo (Schumann et al., 2006; Wei et al., 2006). Of potential interest, the sphingosine chain of  $\alpha$ -GalCer interacts with Leu84 of mCD1d, a residue that packs against Leu99 $\alpha$  of the CDR3 $\alpha$  loop, the position of which and extent of mCD1d contacts was differentially influenced by the V $\beta$ 8.2 and V $\beta$ 7 usage. Accordingly, it suggests that different length lipid tails may alter the Leu84-CDR3 $\alpha$  loop contact, thereby providing a subtle mechanism for NKT TCRs to “sense” various ligands differently (McCarthy et al., 2007). In this regard, improving the resolution of the human NKT TCR-CD1d- $\alpha$ -GalCer complex from 3.2 Å to 2.5 Å resolution is important, because it will serve as a more accurate benchmark to evaluate the subtle effects differing ligands may impart on the conformation of the CD1d Ag-binding cleft, which in turn may effect NKT TCR recognition. Plasticity in the NKT TCR-CD1d interaction is also suggested by the altered positioning of the  $\alpha$ -GalCer head group between the human and mouse CD1d structures (Godfrey et al., 2005). Although reciprocal cross species reactivity is observed between the V $\beta$ 8.2 and V $\beta$ 11 NKT TCR, this is partly diminished in the V $\beta$ 7 NKT TCR. In addition, the  $\alpha$ -GalCer head group bound to mCD1d was observed to be shifted when ligated to the mouse NKT TCRs, which suggests that flexibility in the sugar head group may play a role in the NKT TCR recognition of other Ags, such as the bulky iGb3. Flexibility in the peptide Ag has also been observed in a TCR-pMHC interaction (Tynan et al., 2007). Indeed, a basic superposition of the mCD1d-iGb3 structure (Zajonc et al., 2008) onto our V $\beta$ 8.2 NKT TCR-CD1d- $\alpha$ -GalCer structure indicates that such flexibility may occur, unless a significantly different binding mode exists between V $\beta$ 8.2 NKT TCR-mCD1d- $\alpha$ -GalCer and V $\beta$ 8.2 NKT TCR-mCD1d-iGb3, which seems less likely with the mutagenesis data that suggest a similar docking mode for iGb3 and  $\alpha$ -GalCer (Mallevaey et al., 2009; Scott-Browne et al., 2007).

The different NKT TCR $\beta$  chains reported here converge on a common CD1d-antigen footprint, yet differences within these footprints were evident. Thus, although the NKT TCR could be considered as a pattern recognition receptor, our study reveals the potential for greater diversity at the NKT TCR-CD1d interface, thus providing greater scope for the differential recognition of a broad variety of CD1d-restricted antigens.

## EXPERIMENTAL PROCEDURES

### Cloning and Expression of Genes Encoding the Mouse NKT V $\alpha$ 14, V $\beta$ 8.2, and V $\beta$ 7 TCRs

RNA was extracted from NKT-expressing mouse thymocytes (purified by flow cytometric sorting of thymocytes stained with CD1d- $\alpha$ -GalCer tetramers) and reverse transcribed. cDNAs encoding each the mouse NKT V $\alpha$ 14, V $\beta$ 8.2, and V $\beta$ 7 NKT TCRs were amplified by PCR and cloned into P-GEM Easy (Promega). We were unable to refold the intact ectodomains of mouse TCRs (data not shown) and employed the use of the human constant domains of the NKT TCR to aid in refolding. In brief, soluble chimeric mouse-human TCR gene segments were then PCR generated by splicing by overlap extension and transferred into the expression vector PET30 (Novagen). Stop codons were inserted immediately before the codons encoding the cysteines naturally forming alpha-beta interchain disulfide bonds. Instead, interchain disulfide pairing was achieved through Thr48Cys and Ser57Cys mutations introduced into the human alpha and beta constant domains, respectively. Each chimeric gene was thus predicted to encode a soluble hybrid mouse-human NKT TCR consisting of a mouse variable and a human constant domain, lacking a transmembrane and cytoplasmic domain.

Soluble V $\alpha$ 14-V $\beta$ 8.2 and V $\alpha$ 14-V $\beta$ 7 NKT TCRs were expressed in BL21 *E. coli*, and inclusion body protein was prepared, refolded, and purified as per the protocol of Garboczi et al. (1996), except protein was refolded in the presence of either 1 M (V $\alpha$ 14 and V $\beta$ 8.2) or 5 M (V $\alpha$ 14 and V $\beta$ 7) urea. The functional integrity of the NKT TCRs was confirmed by gel filtration, gel shift experiments, and anti-TCR mAb ELISA reactivity (Figure S1).

### Expression and Purification of CD1d

mCD1d was produced in-house as described previously (Matsuda et al., 2000). In brief, mCD1d was made with a dual promoter baculovirus transfer vector, pBacp10pH, kindly provided by M. Kronenberg (La Jolla Institute for Allergy and Immunology, CA). Recombinant mCD1d was produced with a BirA tag followed by a 6 amino acid histidine tag and expressed with HI5 insect cells. Soluble mCD1d protein was purified with Ni-Agarose affinity purification and subsequently passed over a Superdex 200 16/60 gel filtration column to remove aggregated material. For making mCD1d tetramers or for coating Bio-Rad ProteOn chips, purified mCD1d was biotinylated with BirA enzyme (Avidity) as per manufacturer's protocol. The BirA and His-tag were not removed prior to crystallization. Human CD1d was made in an analogous manner, with the exception that it lacked a BirA tag. Human CD1d was biotinylated by biotin-maleimide treatment of a free cysteine residue at the C-terminal end.

### Loading of CD1d

Loading of CD1d was carried out by incubating with  $\alpha$ -GalCer (provided by Kirin Brewery Co. and Alexis Biochemicals) in a 3:1 (lipid:protein) molar ratio at room temperature overnight. Excess  $\alpha$ -GalCer was removed from CD1d via Superdex 200 10/300 gel filtration.

### Complexation of NKT TCRs with CD1d- $\alpha$ -GalCer

Purified NKT TCR and  $\alpha$ -GalCer-loaded CD1d were mixed, and the ternary complex was isolated by gel filtration on a Superdex 200 16/60 column (GE Healthcare), concentrated to 10 mg/ml, and used in crystal trials.

### Flow Cytometry and CD1d- $\alpha$ -GalCer Tetramer Inhibition Assay

Anti-mouse TCR $\beta$ -allophycocyanin (APC) (clone H57-597) and CD3-APC (clone 145-2C11) were purchased from BD Biosciences. The CD1d- $\alpha$ -GalCer tetramer inhibition assay was carried out as described previously (Kjer-Nielsen et al., 2006). Thymocytes were prepared by gently grinding the organ between frosted glass slides. Stained cells were analyzed by flow cytometry with a FACScalibur flow cytometer (Becton Dickinson).

### Crystallization, Structure Determination, and Refinement

The V $\beta$ 8.2 NKT TCR-CD1d- $\alpha$ -GalCer (7 mg/ml in 10 mM Tris [pH 8.0] and 150 mM NaCl) and V $\beta$ 7 NKT TCR-CD1d- $\alpha$ -GalCer (6 mg/ml in 10 mM Tris [pH 8.0] and 150 mM NaCl) complex crystallized at room temperature in 17% polyethylene glycol 10K, 0.1 M ammonium acetate, 0.1 M BisTris (pH 5.5) via the hanging drop vapor diffusion technique. Equal ratio of the protein to mother liquor resulted in plate-like crystals after 2–3 days. The crystals were flash frozen prior to data collection in mother liquor containing 20% glycerol as the cryoprotectant. The crystals of V $\beta$ 8.2 NKT TCR-CD1d- $\alpha$ -GalCer and V $\beta$ 7 NKT TCR-CD1d- $\alpha$ -GalCer complex diffracted to 2.9 Å and 2.8 Å, respectively, and belong to the space group P2<sub>1</sub>2<sub>1</sub>2<sub>1</sub>, with one ternary complex in the asymmetric unit. The human NKT TCR-CD1d- $\alpha$ -GalCer (10 mg/ml in 10 mM Tris [pH 8.0] and 150 mM NaCl) complex crystallized at room temperature in 10%–12% PEG 10K, 0.2 M magnesium chloride, 0.1 M Tris (pH 9.0). The crystals were equilibrated in the precipitation solution with increasing concentrations of PEG 10K to 35% for at least a few days. The dehydrated crystals were flash frozen in the dehydration solution prior to data collection. The human NKT TCR-CD1d- $\alpha$ -GalCer diffracted to 2.5 Å resolution and belong to the space group P2 with two ternary complexes in the asymmetric unit.

Data for the two mouse NKT TCR complexes were collected at the Australian Synchrotron Facility in Melbourne, Australia, and processed with programs from the CCP4 suite (CCP4, 1994). The data for the human NKT TCR-CD1d- $\alpha$ -GalCer were collected at the Advanced Photon Source synchrotron facility in Chicago and processed with HKL2000 and programs from the CCP4 suite. The crystal structure of the V $\beta$ 8.2 NKT TCR-CD1d- $\alpha$ -GalCer was solved by the molecular replacement method with the program Phaser from the CCP4 Suite. The structure of mouse CD1d-glycosphingolipid



complex (Protein Data Bank ID code 2FIK) minus the lipid and the structure of unliganded semi-invariant V $\alpha$ 14 TCR (Protein Data Bank ID code 2Q86) were used as the search models for solving V $\beta$ 8.2 NKT TCR-CD1d- $\alpha$ -GalCer. Refmac in CCP4 suite was used for the initial round of rigid body refinement and subsequently restrained refinement interspersed with rounds of model building with Coot (Emsley and Cowtan, 2004). At a later stage of refinement, restrained refinement included translation libration screw parameters. The progress of refinement was monitored by the  $R_{\text{free}}$  value. The V $\beta$ 7 NKT TCR-CD1d- $\alpha$ -GalCer was solved by the molecular replacement method in Phaser, with V $\beta$ 8.2 NKT TCR-CD1d- $\alpha$ -GalCer minus the lipid as the search model. Initially, the structure was refined via rigid body refinement in Refmac followed by the simulated annealing protocol implemented in Phenix (Zwart et al., 2008). The model was improved with iterative rounds of refinement and model building. Translation libration screw parameters were included at a later stage of refinement and the progress of refinement was monitored by the  $R_{\text{free}}$  value. The human NKT TCR-CD1d- $\alpha$ -GalCer was solved by molecular replacement method in Phaser, with the 3.2 Å structure solved previously (Protein Data Bank ID code 2PO6) minus the lipid as the search model. The quality of the three structures was assessed with the programs within CCP4. The residues that could not be modeled in the V $\beta$ 8.2 NKT TCR-CD1d- $\alpha$ -GalCer were: CD1d, residues 1–7, 90–93, and 110; TCR $\alpha$  chain, residues 134–135 and 209–210; and TCR $\beta$  chain, residues 1–2 and 98–105 (CDR3 $\beta$ ). The residues that could not be modeled in the V $\beta$ 7 NKT TCR-CD1d- $\alpha$ -GalCer were: CD1d, residues 1–7, 88–94, and 108–110; TCR $\alpha$  chain, residues 130–135, 186–187, and 208–210; and TCR $\beta$  chain, residues 1 and 122. The residues that could not be modeled in the human NKT TCR-CD1d- $\alpha$ -GalCer were: CD1d, residues 1–5 for chain A and 1–4 for chain C;  $\beta$ 2 m, residues 98–99 for chain B; TCR $\alpha$  chain, residues 131–132, 137, 154 for chain E and 136 for chain G; and TCR $\beta$  chain, residues 1, 100–101 for chain F and 1 for chain H. For data collection and refinement statistics, see Table S1. All molecular graphics representations were created with PyMol (DeLano, 2002).

### Surface Plasmon Resonance

The interaction between soluble, recombinant CD1d and wild-type and mutant NKT TCRs were analyzed by SPR with a Bio-Rad ProteOn XPR36 instrument (Hercules, CA). All experiments were performed at 25°C in a buffer containing 10 mM HEPES (pH 7.4), 150 mM NaCl, and 0.005% Tween-20 (HBS-T). Streptavidin was diluted into 10 mM sodium acetate (pH 4.5), and ~3000 RU was immobilized on all 6 flow cells of a GLC Sensorchip (Bio-Rad) by amine coupling. Biotinylated CD1d was passed over the surface of the chip and ~700 RU was captured by the streptavidin. Flow cells 1 and 2 contained  $\alpha$ -GalCer-loaded mouse and human CD1d, respectively, whereas flow cells 3 and 4 contained empty mouse and human CD1d and served as control cells. Recombinant wild-type and mutant NKT TCR was subjected to size-exclusion chromatography within 24 hr of analysis and the concentration of purified protein estimated by OD280. Wild-type and mutant NKT TCRs were then serially diluted from 5  $\mu$ M to 0.05  $\mu$ M or 1  $\mu$ M to 0.01  $\mu$ M in HBS-T and injected simultaneously over the test and control surfaces at a flow rate of 30  $\mu$ L/min. After subtraction of data from control flow cells, the interactions were analyzed with the ProteOn Manager software version 2.1 (Bio-Rad) and steady-state  $K_D$  values were derived from the equilibrium option of the software package. Kinetic data were derived with the kinetic fit option of the software and data analysis was fitted with the 1:1 Langmuir binding model.

### Probing Conformational Integrity of the Wild-Type and Mutant NKT TCRs

100  $\mu$ L of soluble NKT TCR (5  $\mu$ g/ml) was added to a 96-well ELISA plate (U96 Maxisorp, Nunc) at 4°C for 16 hr. Plates were then blocked with 200  $\mu$ L of PBS/1% BSA at 37°C for 1 hr. Titrated amounts of the conformationally dependent, constant domain-reactive mAb 12H8 were then added, after which HRP-conjugated anti-mouse Ig was added. O-phenylenediamine substrate (Sigma) was added next and the reaction was terminated with HCl, and ELISA plates were read at 492 nm on a Labsystems Multiscan ELISA plate reader.

### ACCESSION NUMBERS

The coordinates of the mouse V $\alpha$ 14J $\alpha$ 18-V $\beta$ 8.2 NKT TCR-CD1d- $\alpha$ -GalCer, mouse V $\alpha$ 14J $\alpha$ 18-V $\beta$ 7 NKT TCR-CD1d- $\alpha$ -GalCer, and the new human

V $\alpha$ 24J $\alpha$ 18-V $\beta$ 11 NKT TCR-CD1d- $\alpha$ -GalCer complex have been deposited in the Protein Data Bank under accession numbers 3HE6, 3HE7, and 3HUJ, respectively.

### SUPPLEMENTAL DATA

Supplemental Data include four figures and three tables and can be found with this article online at [http://www.cell.com/immunity/supplemental/S1074-7613\(09\)00274-X](http://www.cell.com/immunity/supplemental/S1074-7613(09)00274-X).

### ACKNOWLEDGMENTS

We thank the staff at the Australian synchrotron and the Advance Photon Source (Chicago, IL) for assistance with data collection. The Australian Research Council (ARC), the National Health and Medical Research Council of Australia (NHMRC), and the Cancer Council of Victoria supported this research. L.G. was supported by an NIH grant (AI057485). D.I.G. and M.J.S. are supported by NHMRC Research Fellowships. J.R. is supported by an ARC Federation Fellowship.

Received: December 1, 2008

Revised: April 1, 2009

Accepted: April 24, 2009

Published online: July 9, 2009

### REFERENCES

- Bendelac, A., Savage, P.B., and Teyton, L. (2007). The biology of NKT cells. *Annu. Rev. Immunol.* 25, 297–336.
- Benlagha, K., Weiss, A., Beavis, A., Teyton, L., and Bendelac, A. (2000). In vivo identification of glycolipid antigen-specific T cells using fluorescent CD1d tetramers. *J. Exp. Med.* 191, 1895–1903.
- Borg, N.A., Wun, K.S., Kjer-Nielsen, L., Wilce, M.C., Pellicci, D.G., Koh, R., Besra, G.S., Bharadwaj, M., Godfrey, D.I., McCluskey, J., and Rossjohn, J. (2007). CD1d-lipid-antigen recognition by the semi-invariant NKT T-cell receptor. *Nature* 448, 44–49.
- Brigl, M., van den Elzen, P., Chen, X., Meyers, J.H., Wu, D., Wong, C.H., Redington, F., Ilarionov, P.A., Besra, G.S., Brenner, M.B., and Gumperz, J.E. (2006). Conserved and heterogeneous lipid antigen specificities of CD1d-restricted NKT cell receptors. *J. Immunol.* 176, 3625–3634.
- Brossay, L., Chioda, M., Burdin, N., Koezuka, Y., Casorati, G., Dellabona, P., and Kronenberg, M. (1998). Cd1d-mediated recognition of an alpha-galactosylceramide by natural killer T cells is highly conserved through mammalian evolution. *J. Exp. Med.* 188, 1521–1528.
- Brutkiewicz, R.R. (2006). CD1d ligands: The good, the bad, and the ugly. *J. Immunol.* 177, 769–775.
- Burdin, N., Brossay, L., Koezuka, Y., Smiley, S.T., Grusby, M.J., Gui, M., Taniguchi, M., Hayakawa, K., and Kronenberg, M. (1998). Selective ability of mouse CD1 to present glycolipids: {alpha}-galactosylceramide specifically stimulates V{alpha}14+ NK T lymphocytes. *J. Immunol.* 161, 3271–3281.
- CCP4 (Collaborative Computational Project, Number 4). (1994). The CCP4 suite: Programs for protein crystallography. *Acta Crystallogr. D Biol. Crystallogr.* 50, 760–763.
- Cui, J.Q., Shin, T., Kawano, T., Sato, H., Kondo, E., Taura, I., Kaneko, Y., Koseki, H., Kanno, M., and Taniguchi, M. (1997). Requirement for V{Alpha}14 Nkt cells in Il-12-mediated rejection of tumors. *Science* 278, 1623–1626.
- Dai, S., Huseby, E.S., Rubtsova, K., Scott-Browne, J., Crawford, F., Macdonald, W.A., Marrack, P., and Kappler, J.W. (2008). Crossreactive T cells spotlight the germline rules for [alpha][beta] T cell-receptor interactions with MHC molecules. *Immunity* 28, 324–334.
- DeLano, W.L. (2002). The PyMOL Molecular Graphics System (San Carlos, CA: DeLano Scientific).
- Emsley, P., and Cowtan, K. (2004). Coot: Model-building tools for molecular graphics. *Acta Crystallogr. D Biol. Crystallogr.* 60, 2126–2132.

- Feng, D., Bond, C.J., Ely, L.K., Maynard, J., and Garcia, K.C. (2007). Structural evidence for a germline-encoded T cell receptor-major histocompatibility complex interaction 'codon'. *Nat. Immunol.* 8, 975–983.
- Fischer, K., Scotet, E., Niemeyer, M., Koebernick, H., Zerrahn, J., Maillet, S., Hurwitz, R., Kursar, M., Bonneville, M., Kaufmann, S.H., and Schaible, U.E. (2004). Mycobacterial phosphatidylinositol mannoside is a natural antigen for CD1d-restricted T cells. *Proc. Natl. Acad. Sci. USA* 101, 10685–10690.
- Gadola, S.D., Dulphy, N., Salio, M., and Cerundolo, V. (2002). V  $\alpha$  24-J  $\alpha$  Q-independent, CD1d-restricted recognition of  $\alpha$ -galactosylceramide by human CD4(+) and CD8  $\alpha$   $\beta$ (+) T lymphocytes. *J. Immunol.* 168, 5514–5520.
- Garboczi, D.N., Utz, U., Ghosh, P., Seth, A., Kim, J., VanTienhoven, E.A., Bidison, W.E., and Wiley, D.C. (1996). Assembly, specific binding, and crystallization of a human TCR- $\alpha$  chain with an antigenic Tax peptide from human T lymphotropic virus type 1 and the class I MHC molecule HLA-A2. *J. Immunol.* 157, 5403–5410.
- Godfrey, D.I., and Kronenberg, M. (2004). Going both ways: Immune regulation via CD1d-dependent NKT cells. *J. Clin. Invest.* 114, 1379–1388.
- Godfrey, D.I., MacDonald, H.R., Kronenberg, M., Smyth, M.J., and Van Kaer, L. (2004). NKT cells: What's in a name? *Nat. Rev. Immunol.* 4, 231–237.
- Godfrey, D.I., McCluskey, J., and Rossjohn, J. (2005). CD1d antigen presentation: Treats for NKT cells. *Nat. Immunol.* 6, 754–756.
- Godfrey, D.I., Rossjohn, J., and McCluskey, J. (2008). The fidelity, occasional promiscuity, and versatility of T cell receptor recognition. *Immunity* 28, 304–314.
- Ishizuka, J., Stewart-Jones, G.B.E., van der Merwe, A., Bell, J.I., McMichael, A.J., and Jones, E.Y. (2008). The structural dynamics and energetics of an immunodominant T cell receptor are programmed by its V $\beta$  domain. *Immunity* 28, 171–182.
- Kinjo, Y., Wu, D., Kim, G., Xing, G.W., Poles, M.A., Ho, D.D., Tsuji, M., Kawahara, K., Wong, C.H., and Kronenberg, M. (2005). Recognition of bacterial glycosphingolipids by natural killer T cells. *Nature* 434, 520–525.
- Kinjo, Y., Tupin, E., Wu, D., Fujio, M., Garcia-Navarro, R., Benhnia, M.R., Zajonc, D.M., Ben-Menachem, G., Ange, G.D., Painter, G.F., et al. (2006). Natural killer T cells recognize diacylglycerol antigens from pathogenic bacteria. *Nat. Immunol.* 7, 978–986.
- Kinjo, Y., Pei, B., Bufali, S., Raju, R., Richardson, S.K., Imamura, M., Fujio, M., Wu, D., Khurana, A., Kawahara, K., et al. (2008). Natural sphingomonas glycolipids vary greatly in their ability to activate natural killer T cells. *Chem. Biol.* 15, 654–664.
- Kjer-Nielsen, L., Clements, C.S., Purcell, A.W., Brooks, A.G., Whisstock, J.C., Burrows, S.R., McCluskey, J., and Rossjohn, J. (2003). A structural basis for the selection of dominant  $\alpha$   $\beta$  T cell receptors in antiviral immunity. *Immunity* 18, 53–64.
- Kjer-Nielsen, L., Borg, N.A., Pellicci, D.G., Beddoe, T., Kostenko, L., Clements, C.S., Williamson, N.A., Smyth, M.J., Besra, G.S., Reid, H.H., et al. (2006). A structural basis for selection and cross-species reactivity of the semi-invariant NKT cell receptor in CD1d/glycolipid recognition. *J. Exp. Med.* 203, 661–673.
- Koch, M., Stronge, V.S., Shepherd, D., Gadola, S.D., Mathew, B., Ritter, G., Fersht, A.R., Besra, G.S., Schmidt, R.R., Jones, E.Y., and Cerundolo, V. (2005). The crystal structure of human CD1d with and without  $\alpha$ -galactosylceramide. *Nat. Immunol.* 6, 819–826.
- Mallevaey, T., Scott-Browne, J.P., Matsuda, J.L., Young, M.H., Pellicci, D.G., Patel, O., Thakur, M., Kjer-Nielsen, L., Richardson, S.K., Cerundolo, V., et al. (2009). T cell receptor CDR2 $\beta$  and CDR3 $\beta$  loops collaborate functionally to shape the iNKT cell repertoire. *Immunity* 31, this issue, 60–71.
- Matsuda, J.L., Gapin, L., Fazilleau, N., Warren, K., Naidenko, O.V., and Kronenberg, M. (2001). Natural killer T cells reactive to a single glycolipid exhibit a highly diverse T cell receptor beta repertoire and small clone size. *Proc. Natl. Acad. Sci. USA* 98, 12636–12641.
- Matsuda, J.L., Naidenko, O.V., Gapin, L., Nakayama, T., Taniguchi, M., Wang, C.-R., Koezuka, Y., and Kronenberg, M. (2000). Tracking the response of natural killer T cells to a glycolipid antigen using CD1d tetramers. *J. Exp. Med.* 192, 741–754.
- Matsuda, J.L., Mallevaey, T., Scott-Browne, J., and Gapin, L. (2008). CD1d-restricted iNKT cells, the 'Swiss-Army knife' of the immune system. *Curr. Opin. Immunol.* 20, 358–368.
- Mattner, J., Debord, K.L., Ismail, N., Goff, R.D., Cantu, C., 3rd, Zhou, D., Saint-Mezard, P., Wang, V., Gao, Y., Yin, N., et al. (2005). Exogenous and endogenous glycolipid antigens activate NKT cells during microbial infections. *Nature* 434, 525–529.
- McCarthy, C., Shepherd, D., Fleire, S., Stronge, V.S., Koch, M., Illarionov, P.A., Bossi, G., Salio, M., Denkberg, G., Reddington, F., et al. (2007). The length of lipids bound to human CD1d molecules modulates the affinity of NKT cell TCR and the threshold of NKT cell activation. *J. Exp. Med.* 204, 1131–1144.
- Porcelli, S., Yockey, C.E., Brenner, M.B., and Balk, S.P. (1993). Analysis of T cell antigen receptor (TCR) expression by human peripheral blood CD4–8- $\alpha$ / $\beta$  T cells demonstrates preferential use of several V  $\beta$  genes and an invariant TCR  $\alpha$  chain. *J. Exp. Med.* 178, 1–16.
- Rudolph, M.G., Stanfield, R.L., and Wilson, I.A. (2006). How TCRs bind MHCs, peptides, and coreceptors. *Annu. Rev. Immunol.* 24, 419–466.
- Schumann, J., Voyle, R.B., Wei, B.Y., and MacDonald, H.R. (2003). Cutting edge: Influence of the TCR V $\beta$  domain on the avidity of CD1d: $\alpha$ -galactosylceramide binding by invariant V $\alpha$ 14 NKT cells. *J. Immunol.* 170, 5815–5819.
- Schumann, J., Mycko, M.P., Dellabona, P., Casorati, G., and MacDonald, H.R. (2006). Cutting edge: Influence of the TCR V $\beta$  domain on the selection of semi-invariant NKT cells by endogenous ligands. *J. Immunol.* 176, 2064–2068.
- Scott-Browne, J.P., Matsuda, J.L., Mallevaey, T., White, J., Borg, N.A., McCluskey, J., Rossjohn, J., Kappler, J., Marrack, P., and Gapin, L. (2007). Germline-encoded recognition of diverse glycolipids by natural killer T cells. *Nat. Immunol.* 8, 1105–1113.
- Tynan, F.E., Reid, H.H., Kjer-Nielsen, L., Miles, J.J., Wilce, M.C., Kostenko, L., Borg, N.A., Williamson, N.A., Beddoe, T., Purcell, A.W., et al. (2007). A T cell receptor flattens a bulged antigenic peptide presented by a major histocompatibility complex class I molecule. *Nat. Immunol.* 8, 268–276.
- Wei, D.G., Curran, S.A., Savage, P.B., Teyton, L., and Bendelac, A. (2006). Mechanisms imposing the V $\beta$  bias of V $\alpha$ 14 natural killer T cells and consequences for microbial glycolipid recognition. *J. Exp. Med.* 203, 1197–1207.
- Wu, D.Y., Segal, N.H., Sidobre, S., Kronenberg, M., and Chapman, P.B. (2003). Cross-presentation of disialoganglioside GD3 to natural killer T cells. *J. Exp. Med.* 198, 173–181.
- Wun, K.S., Borg, N.A., Kjer-Nielsen, L., Beddoe, T., Koh, R., Richardson, S.K., Thakur, M., Howell, A.R., Scott-Browne, J.P., Gapin, L., et al. (2008). A minimal binding footprint on CD1d-glycolipid is a basis for selection of the unique human NKT TCR. *J. Exp. Med.* 205, 939–949.
- Zajonc, D.M., Cantu, C., 3rd, Mattner, J., Zhou, D., Savage, P.B., Bendelac, A., Wilson, I.A., and Teyton, L. (2005). Structure and function of a potent agonist for the semi-invariant natural killer T cell receptor. *Nat. Immunol.* 6, 810–818.
- Zajonc, D.M., Savage, P.B., Bendelac, A., Wilson, I.A., and Teyton, L. (2008). Crystal structures of mouse CD1d-iGb3 complex and its cognate V $\alpha$ 14 T cell receptor suggest a model for dual recognition of foreign and self glycolipids. *J. Mol. Biol.* 377, 1104–1116.
- Zhou, D., Mattner, J., Cantu, C., 3rd, Schrantz, N., Yin, N., Gao, Y., Sagiv, Y., Hudspeth, K., Wu, Y.P., Yamashita, T., et al. (2004). Lysosomal glycosphingolipid recognition by NKT cells. *Science* 306, 1786–1789.
- Zwart, P.H., Afonine, P.V., Grosse-Kunstleve, R.W., Hung, L.-W., Ioerger, T.R., McCoy, A.J., McKee, E., Moriarty, N.W., Read, R.J., Sacchettini, J.C., et al. (2008). Automated Structure Solution with the PHENIX Suite. *Methods Mol. Biol.* 426, 419–435.